Article

Cell Metabolism

Actomyosin-Mediated Tension Orchestrates Uncoupled Respiration in Adipose Tissues

Graphical Abstract

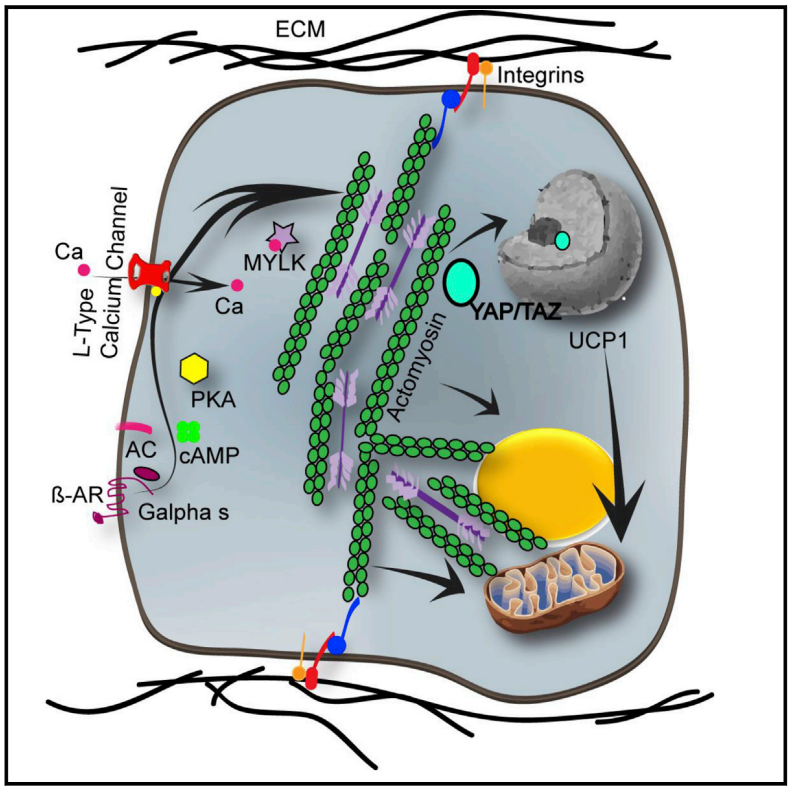

Authors

Kevin M. Tharp, Michael S. Kang, Greg A. Timblin, ..., Kaoru Saijo, Sanjay Kumar, Andreas Stahl

Correspondence

astahl@berkeley.edu

In Brief

Tharp et al. show that brown adipocytes engage tensional actomyosin machinery, similar to muscle tissues, following adrenergic stimulation to mediate the thermogenic program and normal BAT function. These effects are mechanistically mediated through the YAP/TAZ pathway and, on a broad level, highlight the importance of cellular mechanics for cell metabolism.

Highlights

- BAT adrenergic stimulation induces an actomyosin-based mechanical response
- Modulation of actomyosin responses alters oxidative metabolism in adipocytes
- Thermogenic gene expression in adipocytes is in part regulated by YAP/TAZ

Tharp et al., 2018, Cell Metabolism *27*, 602–615
March 6, 2018 © 2018 Elsevier Inc.
https://doi.org/10.1016/j.cmet.2018.02.005

CellPress

CellPress

Cell Metabolism
Article

Actomyosin-Mediated Tension Orchestrates Uncoupled Respiration in Adipose Tissues

Kevin M. Tharp,[1,2] Michael S. Kang,[3] Greg A. Timblin,[4] Jon Dempersmier,[1] Garret E. Dempsey,[1] Peter-James H. Zushin,[1] Jaime Benavides,[1] Catherine Choi,[1] Catherine X. Li,[1] Amit K. Jha,[2] Shingo Kajimura,[5,6] Kevin E. Healy,[2,3,7] Hei Sook Sul,[1] Kaoru Saijo,[4] Sanjay Kumar,[2,3,8] and Andreas Stahl[1,9,*]

[1]Program for Metabolic Biology, Department of Nutritional Sciences and Toxicology, University of California, Berkeley, Berkeley, CA 94720, USA
[2]Department of Bioengineering, University of California, Berkeley, Berkeley, CA 94720, USA
[3]UC Berkeley-UCSF Graduate Program in Bioengineering, University of California, Berkeley, Berkeley, CA 94720, USA
[4]Department of Molecular and Cell Biology, University of California, Berkeley, Berkeley, CA 94720, USA
[5]Diabetes Center, University of California, San Francisco, San Francisco, CA 94143, USA
[6]Department of Cell and Tissue Biology, University of California, San Francisco, San Francisco, CA 94143, USA
[7]Department of Materials Science and Engineering, University of California, Berkeley, Berkeley, CA 94720, USA
[8]Department of Chemical and Biomolecular Engineering, University of California, Berkeley, Berkeley, CA 94720, USA
[9]Lead Contact
*Correspondence: astahl@berkeley.edu
https://doi.org/10.1016/j.cmet.2018.02.005

SUMMARY

The activation of brown/beige adipose tissue (BAT) metabolism and the induction of uncoupling protein 1 (UCP1) expression are essential for BAT-based strategies to improve metabolic homeostasis. Here, we demonstrate that BAT utilizes actomyosin machinery to generate tensional responses following adrenergic stimulation, similar to muscle tissues. The activation of actomyosin mechanics is critical for the acute induction of oxidative metabolism and uncoupled respiration in UCP1$^+$ adipocytes. Moreover, we show that actomyosin-mediated elasticity regulates the thermogenic capacity of adipocytes via the mechanosensitive transcriptional co-activators YAP and TAZ, which are indispensable for normal BAT function. These biomechanical signaling mechanisms may inform future strategies to promote the expansion and activation of brown/beige adipocytes.

INTRODUCTION

Brown and beige adipose tissues (BATs) are critical for thermoregulation by uncoupling oxidative phosphorylation through the action of uncoupling protein 1 (UCP1). Brown adipose is innate, whereas beige adipose is adaptive and arises from the *trans*-differentiation of white adipocytes or *de novo* from mesenchymal stem cells (MSCs) residing in white adipose tissues (WATs) (Bartelt and Heeren, 2014; Harms and Seale, 2013; Kajimura et al., 2015). Interestingly, both brown and beige adipocytes have been described to possess muscle-like origins and characteristics. Brown adipocytes express muscle-specific genes (Timmons et al., 2007; Walden et al., 2009), possess a mitochondrial proteome more reminiscent of myocytes than adipocytes (Forner et al., 2009), and are enriched for transcription factors critical for muscle development prior to differentiation (Seale et al., 2008). Beige adipocytes have been found to share similarities with vascular smooth muscle (Berry et al., 2016; Long et al., 2014), which brown adipocytes do not. Importantly, the transcriptional co-regulator PRDM16 (Seale et al., 2008; Wang and Seale, 2016) biases these mesenchymal precursor cells toward adipogenesis rather than myogenesis, despite their otherwise myocytic expression profiles. Overall, it appears that the expression of UCP1 is variable depending on which precursors or adipocytes are exposed to a given stimulus.

Adipogenesis encompasses transformative cytoskeletal rearrangements thought to facilitate intracellular accumulation of lipids (Gregoire et al., 1998). However, these cytoskeletal rearrangements are now recognized as critical components of the adipogenic program that facilitate myocardin-related transcription factor A (MRTFA) nuclear exclusion (McDonald et al., 2015; Nobusue et al., 2014). MRTFA binds G-actin during cytoskeletal remodeling, thereby preventing its function as a serum response factor (SRF) co-factor (Miralles et al., 2003; Olson and Nordheim, 2010; Posern and Treisman, 2006), which promotes adipogenic gene expression requisite for differentiation. Interestingly, alterations in actomyosin structure can alter cellular elasticity, which plays a major role in the differentiation of MSCs (Engler et al., 2006; McBeath et al., 2004; Sordella et al., 2003). Mechanosensitive transcriptional co-activators, yes-associated protein 1/WW domain-containing transcription regulator protein 1 (YAP/TAZ), regulate growth and differentiation of mesenchymal precursors in response to extracellular matrix and cytoskeletal tension (Dupont et al., 2011; Halder et al., 2012; Hansen et al., 2015; Hong et al., 2005; Moroishi et al., 2015a).

The conspicuous morphological differences between white and brown/beige adipocytes imply significant differences in cytoskeletal structure, composition, and dynamics. Thermogenic adipocytes maintain an extensive cytoskeletal network

that supports and organizes multilocular lipid droplets and numerous mitochondria, whereas white adipocytes are comprised of a unilocular lipid droplet. Surprisingly, the functional differences of these BAT versus WAT cytoskeletal structures and organizations have yet to be characterized. Previous tissue engineering efforts led us to measure the mechanical properties of adipose depots, where we noticed that BAT possesses a higher storage modulus than WAT (Tharp and Stahl, 2015). Due to the fact that BATs possess muscle-like physical properties and express muscle-specific cytoskeletal components, we hypothesized that brown/beige adipose generates cytoskeletal stiffness requisite to maintain or promote differentiation status. In addition, since muscular actomyosin contraction and cellular stiffness can be regulated by adrenergic signaling (Bers, 2002), which also serves as a critical cold-inducible signaling pathway in BAT (Cannon and Nedergaard, 2004; Harms and Seale, 2013; Inagaki et al., 2016), we postulated that adrenergic stimulation may promote cellular stiffness in thermogenic adipocytes. Indeed, we report that, in response to adrenergic stimulation, brown adipocytes induce cellular stiffness critical for metabolic activation and uncoupled respiration. In addition, we show that cellular stiffness is critical for the maintenance of UCP1 expression via type II myosin-regulated YAP/TAZ activity in thermogenic adipocytes.

RESULTS

Adrenergic Stimulation Promotes Actomyosin-Mediated Stiffness in BAT

Using parallel plate rheometry on intact/live tissues and decellularized tissues, we characterized the tissue-scale physical differences between BAT and WAT. Intact WAT has a storage modulus (stiffness) of ~3 kPa, whereas that of BAT is ~4.5 kPa (Figure 1A). When the tissues are decellularized (Schulz et al., 2011), the remnant cell-free tissue has a significantly reduced storage modulus. The cellular contribution to modulus is then estimated by subtracting the decellularized tissue modulus from the intact tissue modulus (Figure 1B). Based on this (intact − decellularized) assessment, brown adipocytes collectively generate and/or experience significantly higher mechanical stress than their white adipose counterparts, and the visceral adipose extracellular matrix (ECM) is much less stiff than subcutaneous adipose ECM, possibly due to differences in porosity. Strikingly, cold exposure (4°C) induces elevated stiffness in BAT compared with BAT from mice exclusively housed at room temperature for the same time period (23°C) (Figure 1C).

To determine if this change in tissue stiffness is the product of cellular behavior rather than alterations of ECM mechanical properties, we examined the mechanical response to isoproterenol, an established chemical proxy for cold exposure, with a clonal brown adipose cell line (brown adipocytes) that the Kajimura lab developed previously (Galmozzi et al., 2014). Using atomic force microscopy (AFM) to directly measure cellular stiffness, we found that isoproterenol administration induces a contractile-like response, which initially stiffens the cell cortex followed by transduction of tension to the interior of the cell depicted by AFM force maps of single cells and scanning indentations across the monolayer (Figures 1D and S1A). On a tissue level, BAT explants also respond acutely to isoproterenol with elevated cellular stiffness, reaching its peak 30 min after stimulation (Figure 1E).

An interesting, but largely ignored, aspect of the muscle-like characteristics of BAT is the expression of muscle-specific type II myosin heavy chains (MYH), which are known to facilitate intrinsic physical forces in cells. RNA sequencing (RNA-seq) comparing white adipose with brown adipose has revealed muscle-like characteristics (Figure 1F), which are resistant to high-fat-diet-induced "whitening" (Hill, 2015). When comparing the relative abundance of MYH species in these tissues, it is evident that brown adipose tissue is enriched with MYH1, -2, -4, -7, and -11 expression (Figure S1B). To investigate whether the expression of these myosin species is a product of the differentiation program in UCP1$^+$ adipocytes and not a product of contaminating stromal vascular fraction, we measured their expression in a clonal brown adipose cell line. We found that MYH1, -2, and -4 were not expressed in brown adipocytes, whereas MYH7 expression was induced during differentiation while MYH9 (NMIIa) and MYH10 (NMIIb) remained constant (Figure S1C). Since MYH7 appears to be uniquely expressed in brown adipocytes, we knocked down expression of MYH7 during differentiation and observed a significant reduction of UCP1 expression (Figure 1G). Immunofluorescence microscopy (Figure S1D) and western blots confirm MYH7 protein expression in BAT, which is not detectable in WAT (Figure S1E).

Actomyosin-Mediated Tension Is Critical for Thermogenic Capacity of Adipocytes

To test if actomyosin-mediated tension is critical for the expression of UCP1, we applied two different type II myosin inhibitors, blebbistatin and 2,3-butanedione monoxime (2,3-BDM) (Backx et al., 1994; Hall and Hausenloy, 2016; Kovacs et al., 2004; Limouze et al., 2004; Ostap, 2002; Schiller et al., 2013; Straight et al., 2003), and found significantly reduced expression of UCP1 in BAT explants in terms of mRNA (Figure 2A) and protein (Figure 2B). We then applied these inhibitors to fully differentiated brown adipocytes already expressing levels of UCP1 comparable with BAT, and found that type II myosin inhibition reduced UCP1 expression within 24 hr of treatment (Figure S2A). To determine if tension is a critical regulator of UCP1 expression in beige adipose, we used a white adipose-derived cell line (beige adipocytes) analogous to the brown adipocyte cell line, which expresses high levels of UCP1 upon treatment with rosiglitazone. When UCP1$^+$ beige adipocytes are subjected to actomyosin inhibition, we found an ~70% reduction of UCP1 mRNA expression (Figure S2B). AFM revealed that stiffness in the cytoplasmic regions of brown adipocytes is significantly reduced by blebbistatin and increased by isoproterenol treatment with 24 hr of treatment (Figure S2D), similar to 30 min of treatment (Figure S1A).

Subsequently, we sought to determine what upstream regulators of actomyosin-mediated tension are expressed in adipose. We examined the expression levels of myosin light-chain kinases (MYLKs), serine/threonine kinases that promote type II myosin-mediated contractions (Kamm and Stull, 1985), and found that the predominant MYLK expressed in brown adipocytes was the calcium-sensitive smooth muscle isoform (Figure S2E). Interestingly, Ca^{2+} flux from the endoplasmic reticulum (ER) and extracellular medium is a known response to adrenergic

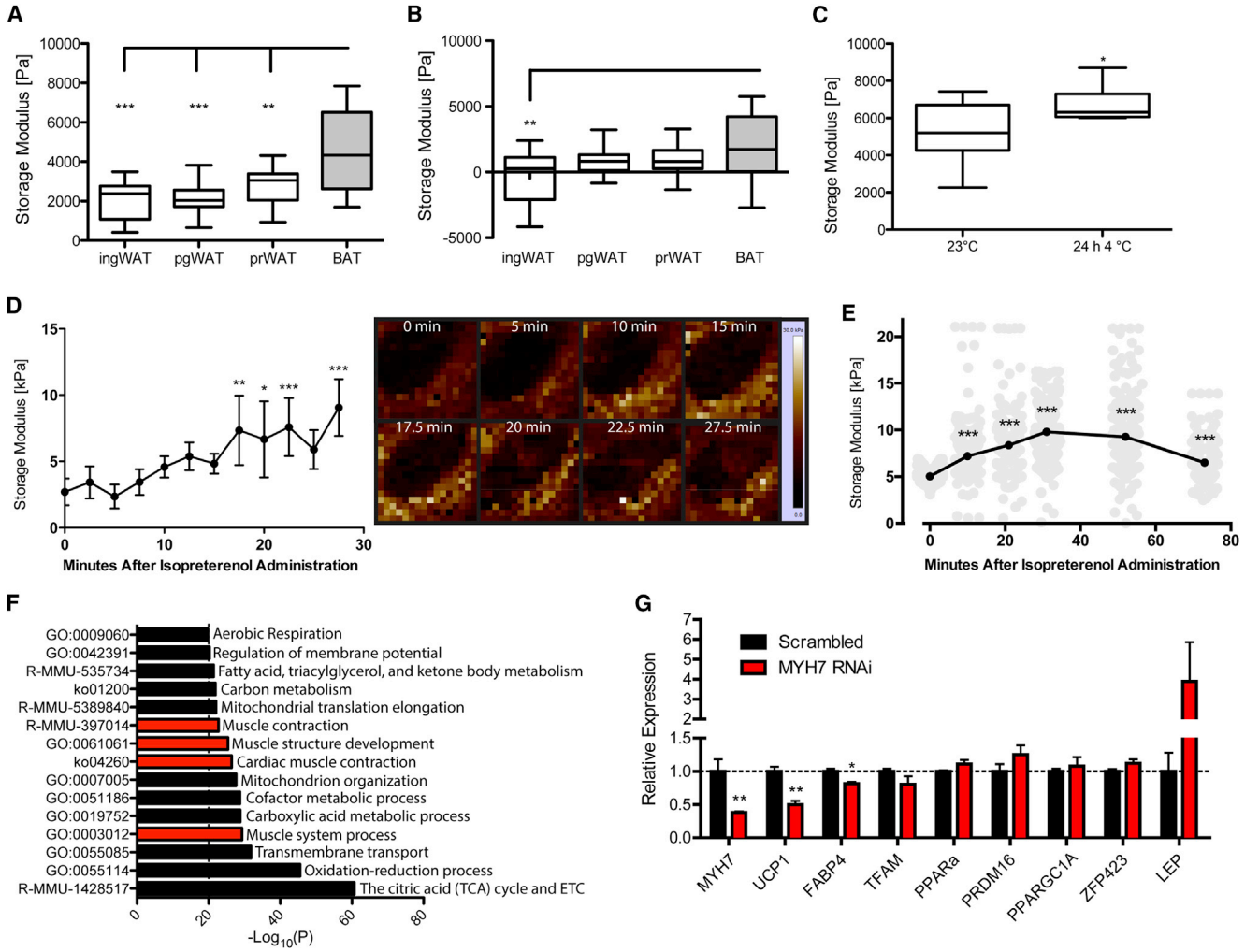

Figure 1. Brown Adipocytes Mechanically Respond to Adrenergic Stimulation

(A) Storage modulus of intact adipose tissues from 16-week-old FVB/NJ mice (inguinal WAT [IngWAT], perigonadal WAT [pgWAT], perirenal WAT [prWAT], and BAT) measured with parallel plate rheometry (n = 16) (8 males and 8 females).

(B) Subtraction of (intact tissue − decellularized tissue), measured with parallel plate rheometry (n = 16) (8 males and 8 females).

(C) Storage modulus of intact BAT from 16-week-old male FVB/NJ mice housed at 23°C or exposed to 24 hr of 4°C before measurement, measured with parallel plate rheometry (n = 8).

(D) Single-cell measurements of isoproterenol-induced stiffness in cultured brown adipocytes with corresponding force map depicting the location of tensional changes in a cell, 30 μm^2 grid measured with atomic force microscopy (AFM) (n = 6).

(E) BAT explant isoproterenol-induced stiffness 100 μM^2 grid measured with AFM, 256 points measured per explant per time point.

(F) Metascape gene ontology analysis of BAT and WAT from 22-week-old C57Bl6/N mice fed a high-fat diet for 14 weeks (n = 4).

(G) Relative mRNA expression of brown adipocytes on day 6 of differentiation transfected with MYH7 RNAi or scrambled RNAi 48 hr prior, RT-PCR (ΔΔCT, normalized to GAPDH) (n = 3).

Error bars represent ± SEM. *p < 0.05, **p < 0.01, and ***p < 0.001. See also Figure S1.

stimulation in brown adipocytes that could initiate MYLK-mediated type II MYH activity (Dolgacheva et al., 2003; Leaver and Pappone, 2002). To determine if MYLK and type II MYH activity play a role in actomyosin-based regulation of UCP1, we applied treatments of ML7 (MYLK inhibitor) and blebbistatin (type II myosin inhibitor) to brown adipocytes with/without isoproterenol for 24 hr and found that, while UCP1 is still induced by isoproterenol (~3-fold), UCP1 expression is lost relative to vehicle controls (Figure 2C). To verify the role of MYLK, we utilized genetic manipulations of MYLK expression during differentiation of brown adipocytes, which results in the loss of UCP1 expression, while PRDM16, PPARG, and FABP4 are significantly upregulated (Figure 2D).

Adrenergic stimulation of $MYH7^+$ cells has been found to induce cytoskeletal tension, cellular elasticity, increased beat rate, and contractile velocity (Bers, 2002). Adrenergic stimulation is also well known to promote thermogenic responses in $UCP1^+$ adipocytes through β-adrenergic receptors. Therefore, we decided to test if actomyosin activity affects the thermogenic capacity of brown adipocytes. Isoproterenol-induced cytoskeletal stiffening is blocked by either co-administration of blebbistatin (Figure 2E) or MYLK knockdown (Figure 2F). In

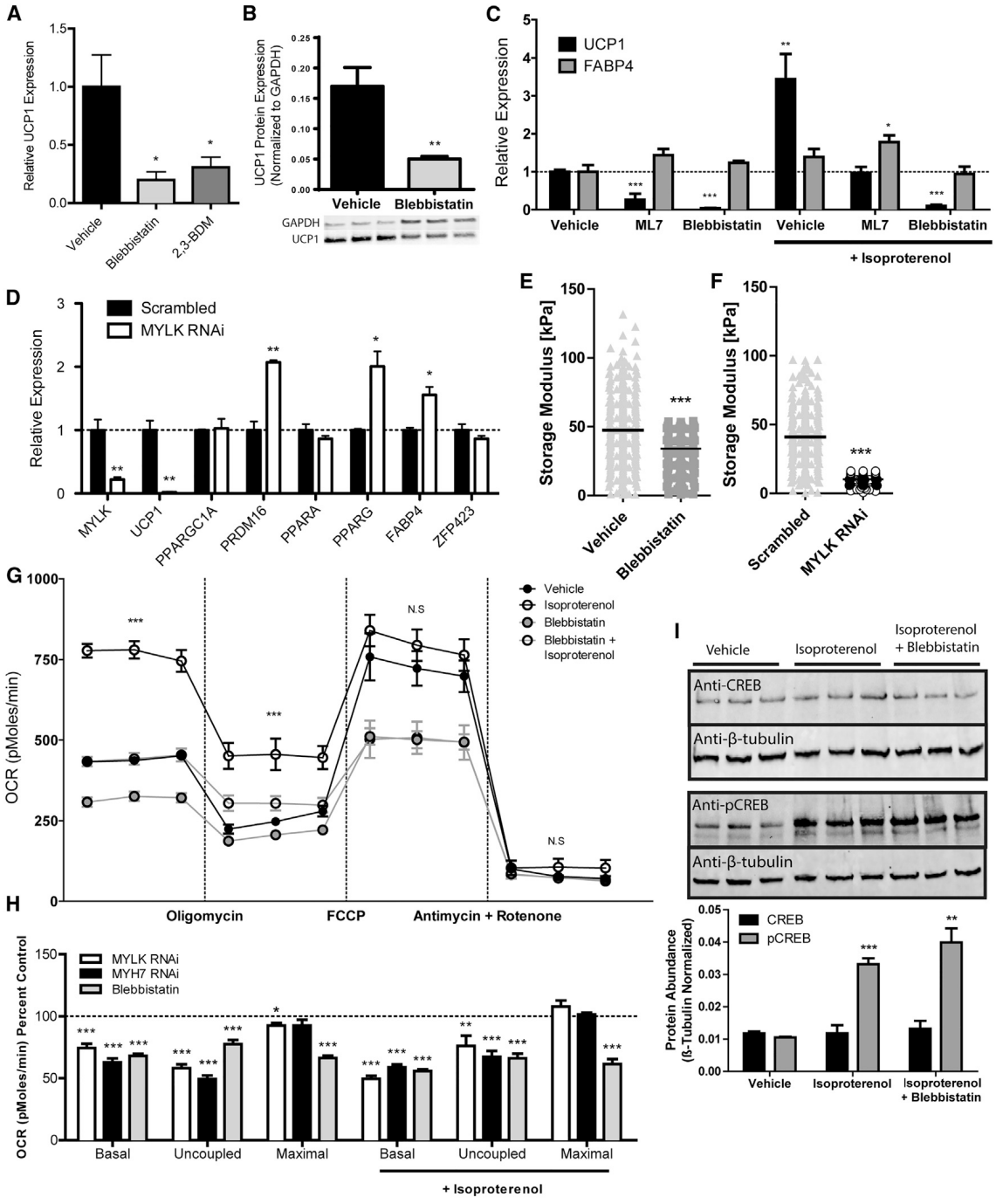

Figure 2. Actomyosin-Mediated Tension is Critical for the Thermogenic Capacity of Adipocytes

(A) Relative UCP1 mRNA expression in BAT explants treated with 100 μM blebbistatin or 1 mM 2,3-butanedione monoxime (2,3-BDM) for 24 hr, RT-PCR (ΔΔCT, normalized to GAPDH) (n = 10).

(B) UCP1 protein expression in BAT explants treated with 100 μM blebbistatin for 24 hr (normalized to GAPDH) (n = 3).

(C) Relative UCP1 and FABP4 mRNA expression in differentiated brown adipocytes treated with ± 1 μM isoproterenol and/or 10 μM ML-7 or 100 μM blebbistatin, 24-hr treatment, RT-PCR (ΔΔCT, normalized to PPIA) (n = 3).

(D) Relative gene expression changes observed in brown adipocytes on day 6 of differentiation transfected with MYLK RNAi or scrambled RNAi 48 hr prior, RT-PCR (ΔΔCT, normalized to GAPDH).

(E) AFM assessment of cellular stiffness across a monolayer of fully differentiated brown adipocytes 30 min after treatment with 1 μM isoproterenol or 1 μM isoproterenol and 100 μM blebbistatin, 100 μM^2 grid measured with AFM, 256 points measured per monolayer.

(F) AFM assessment of cellular stiffness across a monolayer of fully differentiated brown adipocytes 30 min after treatment with 1 μM isoproterenol on day 6 of differentiation transfected with MYLK RNAi or scrambled RNAi 48 hr prior, 100 μM^2 grid measured with AFM, 256 points measured per monolayer.

(legend continued on next page)

brown adipocytes, basal and uncoupled respiration was significantly upregulated by isoproterenol treatment, while co-administration of blebbistatin blocked this metabolic augmentation (Figure 2G). Knockdown of MYLK or MYH7 recapitulated the effects of blebbistatin treatment on unstimulated and isoproterenol-stimulated metabolic capacity, except for the fact that blebbistatin, a comprehensive type II myosin inhibitor, reduced ionophore-mediated maximal respiratory rates, suggesting a critical role for other type II MYH species in mitochondrial maintenance or substrate availability (Hatch et al., 2014; Korobova et al., 2013; Pfisterer et al., 2017) (Figure 2H). However, this effect may be cell-type specific since previous reports have specifically identified blebbistatin as not perturbing mitochondrial respiration in cardiomyocytes *in vitro* (Hall and Hausenloy, 2016).

To verify that blebbistatin treatment did not alter metabolic rate by impeding protein kinase A (PKA) activation, we assessed if the cAMP response element binding protein (CREB) was phosphorylated by PKA in response to adrenergic stimulation in the presence of blebbistatin (Figure 2I). Blebbistatin had no effect on pCREB levels in response to adrenergic stimulation, which is known to promote UCP1 expression (Cao et al., 2004), which in turn explains why UCP1 expression is still induced (~3-fold) by isoproterenol treatment in the presence of ML7 or blebbistatin. However, since global UCP1 expression was dramatically downregulated by blebbistatin or ML7 treatment and through MYLK or MYH7 knockdown, we determined that actomyosin-mediated regulation of UCP1 expression is orthogonal to the known mechanisms of UCP1 regulation.

Targeting Actomyosin Mechanics to Promote Thermogenic Capacity of Brown Adipocytes

In cardiomyocytes, type II myosin-mediated contractions can be generated in response to adrenergic stimulation through PKA-mediated activation of L-type Ca^{2+} channels (CACNA1a-CACNA2d4) (Bers, 2002; Kamp and Hell, 2000), which we found be expressed in BAT from tissue (Figure 1F). The L-type Ca^{2+} channel-mediated influx of calcium stimulates MYLK, which phosphorylates type II myosin hexamers, promoting their assembly into think filaments, association with actin, and ATPase activity, which all enhance actomyosin-based tension.

To test if modulation of this pathway directly alters the function of brown adipocytes *in vitro*, we administered MYH7-potentiator (omecamtiv mecarbil [OM]), myosin ATPase activator (EMD57003), and L-type Ca^{2+} channel inhibitor (verapamil), and induced expression of a constitutively active form of MYLK (CA-MYLK) (Wong et al., 2015) in brown adipocytes (Figure 3A). Treatment with OM alone for 24 hr did not induce UCP1 expression in brown adipocytes, but co-administration with isoproterenol did significantly enhance UCP1 expression relative to isoproterenol treatment alone (Figure S3A). OM, EMD57003, and CA-MYLK expression all potentiated the metabolic rate of brown adipocytes when stimulated with isoproterenol. Interestingly, as has been shown for cardiomyocytes, OM and EMD57003 reduced oxygen consumption in unstimulated conditions thought to be a product of enhanced efficiency of myosin function (Figure 3B), whereas verapamil treatment dramatically reduced metabolic function of brown adipocytes (Figure 3B), supporting the notion that reduced respiratory rates observed with verapamil treatment *in vivo* may be partially due to direct effects on brown adipocytes (Figure 3C). Importantly, verapamil had no effect on the metabolic rates of white adipocytes, as they do not express functional levels of "cardiac-specific" L-type Ca^{2+} channels (Figure S3C). Perturbations to actin polymerization with latrunculin B or jasplakinolide had limited effects (Figure S3D), suggesting that actomyosin-mediated tension, and not actin filament assembly per se, is a critical component of the brown adipocyte's metabolic response to adrenergic stimulation.

We then tested if pharmacological enhancement of MYH7 function had metabolic effects *in vivo*. Mice were treated with a subcutaneous injection of OM directly into the interscapular BAT, which markedly enhanced oxygen consumption 48 hr post-treatment both at room temperature (23°C) and in the cold (4°C) (Figure 3D). This enhanced respiratory rate is remarkable, since OM and other myosin activators (EMD 57003) that bind to this region of MYH7 have been found to not significantly alter oxygen consumption of cardiomyocytes while increasing actomyosin-mediated tension (Hwang and Sykes, 2015; Malik et al., 2011; Radke et al., 2014; Shen et al., 2010; Winkelmann et al., 2015).

Mechanosensitive Activation of YAP/TAZ Drives Thermogenic Activity in Adipocytes

To verify that the downregulation of UCP1 expression in response to actomyosin inhibition was not due to de-differentiation and loss of the adipocyte phenotype, we profiled the expression of FABP4, ZFP423, CIDEA, PRDM16, PPARA, PPARG, PPARGC1A, and TFAM during 24-hr treatments (Figure S4A). We found that these adipogenic markers and mediators were largely induced by blebbistatin. To determine in an unbiased fashion what mediated the loss of UCP1 expression, we utilized RNA-seq to evaluate global transcriptomic changes following actomyosin inhibition. KEGG pathway analysis identified the Hippo signaling pathway (Figure 4A). Specifically, motif analysis revealed robust reductions of genes with promoters under the control of TEAD1, TEAD2, and TEAD4 (Figure 4B). YAP/TAZ are co-factors that associate with varied TEADs to function as

(G) Cellular respirometry of brown adipocytes treated ± 1 μM isoproterenol and ± 100 μM blebbistatin (45 min prior to measurement), oxygen consumption rate (OCR) measured with Seahorse XF24, statistical comparison between vehicle and isoproterenol treatment represented on graph, further statistical comparisons depicted in (G) (n = 5 wells).

(H) Relative OCR of brown adipocytes treated ± 1 μM isoproterenol (45 min prior to measurement) and transfected or treated with MYLK RNAi (48 hr prior to measurement), MYH7 RNAi (48 hr prior to measurement), and 100 μM blebbistatin (45 min prior to measurement). OCR measured with Seahorse XF24, statistical comparison and percent OCR between scrambled RNAi versus MYLK RNAi, scrambled RNAi versus MYH7 RNAi, and vehicle versus blebbistatin ± isoproterenol for each phase of the mitochondrial stress test (n = 5 wells of one example of replicated experiments showing analogous effects).

(I) Western blot analysis of CREB and pCREB in brown adipocytes treated with ± 1 μM isoproterenol for 2 hr with/without prior 22 hr of 100 μM blebbistatin treatment, normalized to β-tubulin, LI-COR Odyssey (n = 3).

Error bars represent ± SEM. *$p < 0.05$, **$p < 0.01$, and ***$p < 0.001$. See also Figure S2.

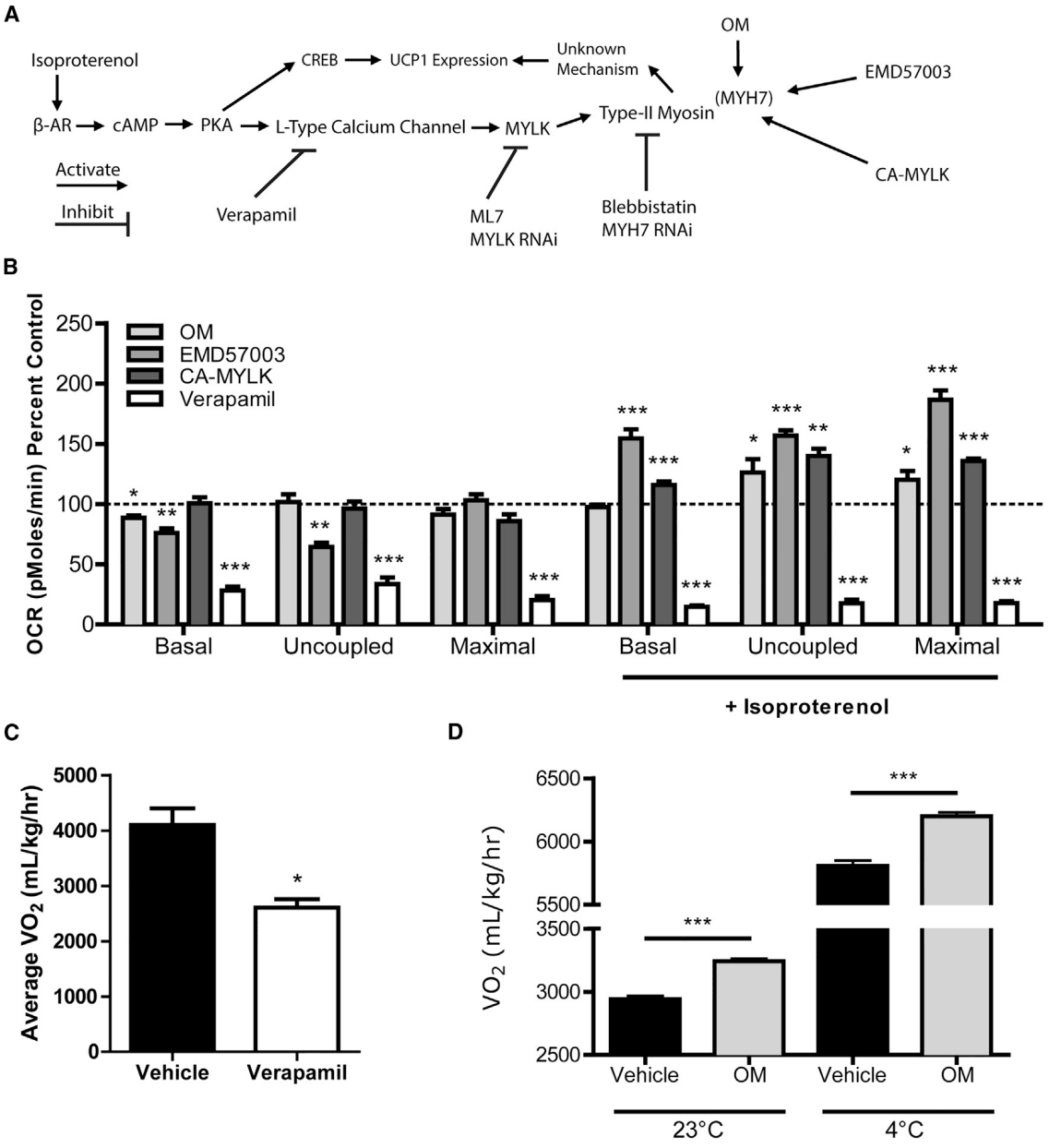

Figure 3. Promoting Actomyosin Mechanics to Promote Thermogenic Capacity of Brown Adipocytes

(A) Schematic depicting adrenergic activation and the subsequent actomyosin-associated targets identified and tested.

(B) Relative OCR of brown adipocytes treated ± 1 μM isoproterenol (45 min prior to measurement) and treated or transfected with 10 μM omecamtiv mecarbil (OM) (45 min prior to measurement), 10 μM EMD57003 (45 min prior to measurement), or CA-MYLK (48 hr prior to measurement). OCR measured with Seahorse XF24, statistical comparison and percent OCR between vehicle versus OM, vehicle versus EMD570033, and empty vector versus CA-MYLK ± isoproterenol for each phase of the mitochondrial stress test (n = 5 wells of one example of replicated experiments showing analogous effects).

(C) Respiratory rate (VO_2) of 16-week-old FVB/NJ injected directly into the subcutaneous interscapular BAT depot with 100 μL of 1 mM OM or vehicle, exposed to ambient temperatures of 4°C and 23°C for 12-hr intervals (n = 5) with no variation in ambulatory parameters observed, measured with temperature controlled Oxymax-CLAMS (Columbus Instruments).

(D) Average respiratory rate (VO_2) over 4 hr of 6-week-old FVB/NJ male mice injected directly into the subcutaneous interscapular BAT depot with 5 mg/kg verapamil (~30 μL) at 23°C (n = 5).

Error bars represent ± SEM. *p < 0.05, **p < 0.01, and ***p < 0.001. See also Figure S3.

the canonical effectors of the Hippo signaling network and mechanosensing pathways to affect cell fate decisions and organ development (Halder et al., 2012; Hansen et al., 2015). Indeed, YAP/TAZ target genes, such as ANKRD1, BIRC5, CYR61, SERPINE1, DLG2, PUMA, WNT10A, BMP4, and CTGF, were all significantly downregulated by blebbistatin treatment (Figures 4A and S4A). Interestingly, MRTFA target genes were not strongly affected (Figure S4A), suggesting that the

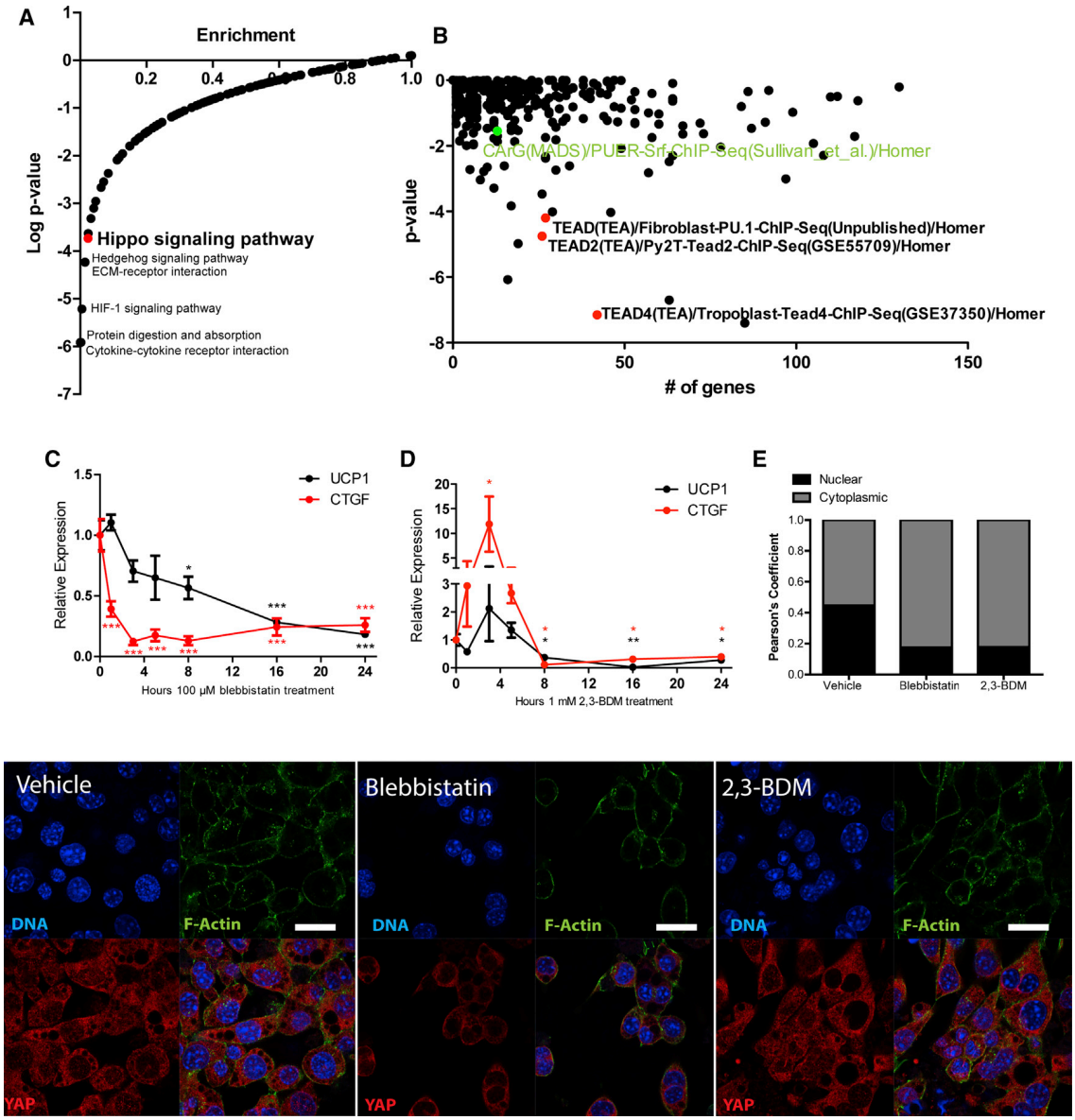

Figure 4. Actomyosin Tension Regulates Mechanosensitive Transcriptional Program

(A) KEGG pathway analysis of genes found by RNA-seq to be significantly downregulated (log2 <1.5 factor) following treatment of differentiated brown adipocytes with 100 μM blebbistatin for 24 hr.

(B) HOMER *de novo* motif analysis showing transcription factor binding sites enriched in promoters of genes significantly downregulated by blebbistatin.

(C) UCP1 and YAP target gene, CTGF, mRNA expression in brown adipocytes treated with 100 μM blebbistatin for 24 hr RT-PCR (ΔΔCT, normalized to GAPDH) (n = 3).

(D) UCP1 and YAP target gene, CTGF, mRNA expression in brown adipocytes treated with 1 mM 2,3-BDM for 24 hr RT-PCR (ΔΔCT, normalized to GAPDH) (n = 3).

(E) Pearson's correlation coefficient of DAPI and YAP analyzed with BitPlane Imaris software from lower-magnification images of the displayed immunofluorescence depicting YAP localization in of brown adipocytes treated with 100 μM blebbistatin or 1 mM 2,3-BDM for 24 hr, YAP (red), F-actin (green), or DAPI (blue). Scale bars, 20 μm.

Error bars represent ± SEM. *p < 0.05, **p < 0.01, and ***p < 0.001. See also Figure S3.

conspicuous regulation of CTGF was primarily through YAP/TAZ rather than MRTFA-SRF (Figure 4B).

Since genes regulated by the Hippo signaling pathway were strongly suppressed by actomyosin inhibition in brown adipocytes, we examined whether or not CTGF was also regulated by blebbistatin or 2,3-BDM (Figures 4C and 4D). Over the course of 24 hr of treatment, CTGF levels trend with UCP1 expression for both blebbistatin and 2,3-BDM. In addition, during the course of brown adipocyte differentiation, CTGF expression increases along with UCP1 (Figure S4B). Given that CTGF expression is a product of YAP/TAZ-associated transcriptional regulation, we used immunofluorescence to determine whether these actomyosin-dysregulating treatments affected YAP nuclear localization in brown adipocytes as they have been extensively shown to

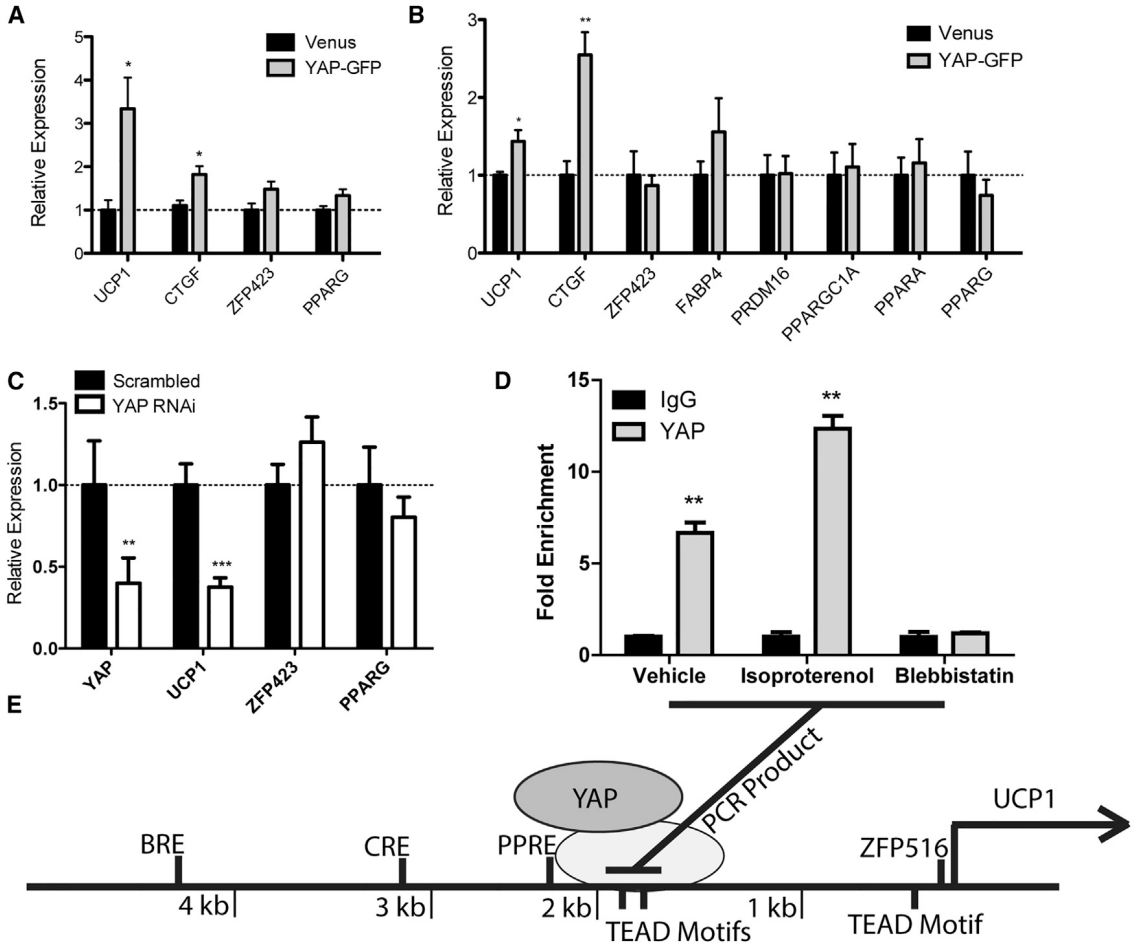

Figure 5. YAP/TAZ Regulates UCP1 Expression in Adipocytes

(A) Gene expression changes observed in differentiated beige adipocytes 24 hr post-transfection with YAP-GFP overexpression construct, RT-PCR (ΔΔCT, normalized to GAPDH) (n = 10).

(B) Gene expression changes observed in differentiated brown adipocytes 24 hr post-transfection with YAP-GFP overexpression construct, RT-PCR (ΔΔCT, normalized to GAPDH) (n = 4).

(C) Gene expression changes observed in differentiated brown adipocytes 24 hr post-transfection with YAP RNAi, RT-PCR (ΔΔCT, normalized to GAPDH) (n = 4).

(D) Chromatin immunoprecipitation (ChIP) of YAP at putative TEAD consensus sequences -1878/-1950 of the UCP1 promoter in brown adipocytes treated with 1 μM isoproterenol for 2 hr or 100 μM blebbistatin for 24 hr.

(E) Schematic representation of the PCR product produced from YAP ChIP-PCR from the UCP1 proximal promoter/enhancer region with the brown fat response element (BRE), cAMP response element (CRE), PPAR response element (PPRE), and ZFP516 binding site depicted (Collins et al., 2010).

Error bars represent ± SEM. *p < 0.05, **p < 0.01, and ***p < 0.001. See also Figure S4.

do so in other cell types (Johnson and Halder, 2014). Unsurprisingly, nuclear YAP localization across 2 mm^2 (Figure 4E) demonstrated impaired nuclear localization via actomyosin inhibition, while isoproterenol treatment enhanced nuclear traffic (Figures S4C and S4D). Surprisingly, blebbistatin did not alter MRTFA localization (Figure S4E), which validates the minimal SRF-MRTFA-associated transcriptional changes that we observed (Figure 4B), and in addition supports the notion that CTGF expression levels are being modulated by YAP/TAZ in this system.

To conclude if endogenous YAP/TAZ transcriptional activity was increased by adrenergic stimulation *in vivo*, we analyzed BAT, inguinal WAT, and perigonadal WAT following a 24-hr 4°C cold challenge and found CTGF and UCP1 significantly upregulated in all of these adipose tissues (Figure S5A). Brown adipocytes treated with isoproterenol *in vitro* also reveal increased CTGF and UCP1 expression (Figure S5B). Impressively, overexpression of YAP in mature beige adipocytes enhanced the already high UCP1 expression, with no significant changes to adipogenic gene expression (Figure 5A) and with a transfection efficiency of around ~15%. Similarly, overexpression of YAP in mature brown adipocytes, with ~15% transfection efficiency, results in significant induction of UCP1 and CTGF mRNA expression 24 hr after transfection (Figure 5B). Overexpression of YAP did not result in any alteration of the expression of ZFP423, FABP4, PRDM16, PPARGC1A, PPARA, or PPARG. To further test if YAP/TAZ is required for UCP1 expression in differentiated brown adipocytes, we knocked down expression of YAP with small interfering RNA (siRNA), which resulted in an ~60% reduction of UCP1 expression while important

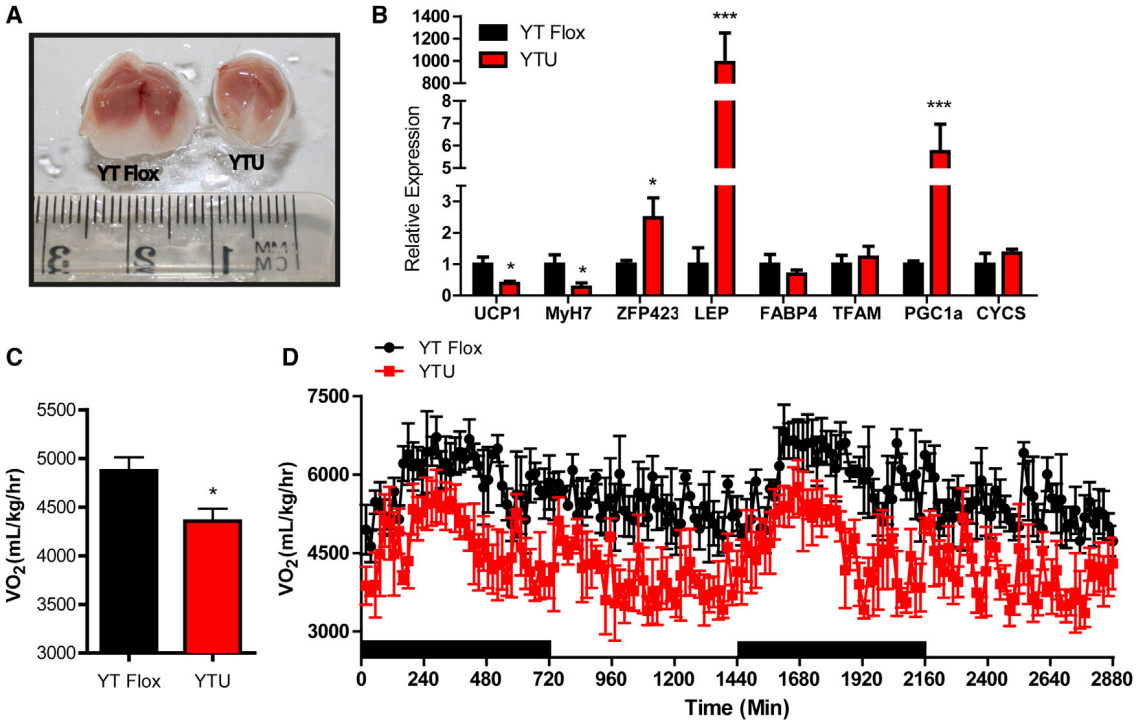

Figure 6. YAP/TAZ Enables Thermogenic Capacity of Adipose Tissue *In Vivo*

(A) Representative photograph of BAT of 4-week-old male YTU and YAP/TAZ flox (YT flox) control mice.

(B) Gene expression observed in 4-week-old male YTU mice, RT-PCR (ΔΔCT, normalized to GAPDH) (n = 4).

(C) Average respiratory rate (VO_2) over 12 hr of 4-week-old male mice at 23°C (n = 4).

(D) Respiratory rate (VO_2) of 4-week-old female mice at 23°C during a 48-hr interval with no variation in ambulatory parameters observed. Average VO_2 p = 0.0444 for 240–720 min (dark) and p = 0.0294 for 720–1,440 min (light), measured with temperature-controlled Oxymax-CLAMS (Columbus Instruments) (n = 3).

Error bars represent ± SEM. *p < 0.05 and ***p < 0.001. See also Figure S5.

adipogenic genes were unaffected (Figure 5C), analogous to what was observed with YAP overexpression. Chromatin immunoprecipitation-qPCR reveals enrichment of YAP −1.8 kb upstream of the UCP1 TSS, a region with two TEAD binding motifs, and this binding is enhanced by isoproterenol and suppressed by blebbistatin treatment (Figures 5D and 5E). To determine if the YAP paralog, TAZ, functions equivalently, and if a specific TEAD is associated with this program, we used siRNA to knock down expression of TAZ and TEAD1–4. We found that TAZ knockdown also resulted in decreased UCP1 expression, and that YAP/TAZ likely coordinates with TEAD1 to mediate effects on UCP1 expression in brown adipocytes (Figure S5C).

YAP/TAZ Enables Thermogenic Capacity of Adipose Tissue

We then sought to clarify the role of YAP/TAZ in BAT function *in vivo* and generated heterozygous $YAP^{fl/+}Taz^{fl/+}$UCP1-Cre^{+} mice (YTU). The reduction in YAP/TAZ expression significantly reduced BAT depot size at 4 weeks of age and yielded a visibly "whitened" appearance (Figure 6A). Whitening of the BAT depots was also apparent on the gene expression level, with leptin expression comparable with WATs as well as reduced UCP1 expression (Figure 6B). The reduced size and UCP1 expression of the BAT from heterozygous YTU mice resulted in impaired metabolic activity of these male and female mice at 4 weeks of age (Figures 6Cand 6D). Due to the compromised metabolic rates observed at 23°C for the 4-week-old YTU mice, we examined the response to cold challenge in 10-week-old YTU mice (Figure S6). Over a 12-hr cold challenge, YTU mice have significantly reduced respiratory rates, suggesting impaired thermoregulation due to the dysregulated BAT.

YTU mice had significantly lower core body temperatures (Figure S7A) and gained body weight more rapidly than control animals on normal chow diets fed *ad libitum* (Figure 7A). This difference in body weight appeared to be exclusively due to increased fat mass, with YTU mice having nearly three times the adiposity of control animals (Figure 7B). At 20 weeks of age, the previously retarded BAT was observed to be significantly more massive than control tissues (Figure 7C), with slightly reduced UCP1 protein expression levels (Figure 7D). Unsurprisingly, the increased BAT mass was due to increased neutral lipid accumulation (Figure 7E) and notably larger adipocytes (Figure S7B). Impressively, on a normal chow diet the YTU mice displayed hyperinsulinemia and reduced glucose tolerance (Figures 7F and 7G).

DISCUSSION

Here, we have identified that β-adrenergic stimulation of brown adipocytes induces cellular stiffness via type II myosins, which acutely facilitates uncoupled respiration while concomitantly promoting thermogenic gene expression. Our findings suggest that

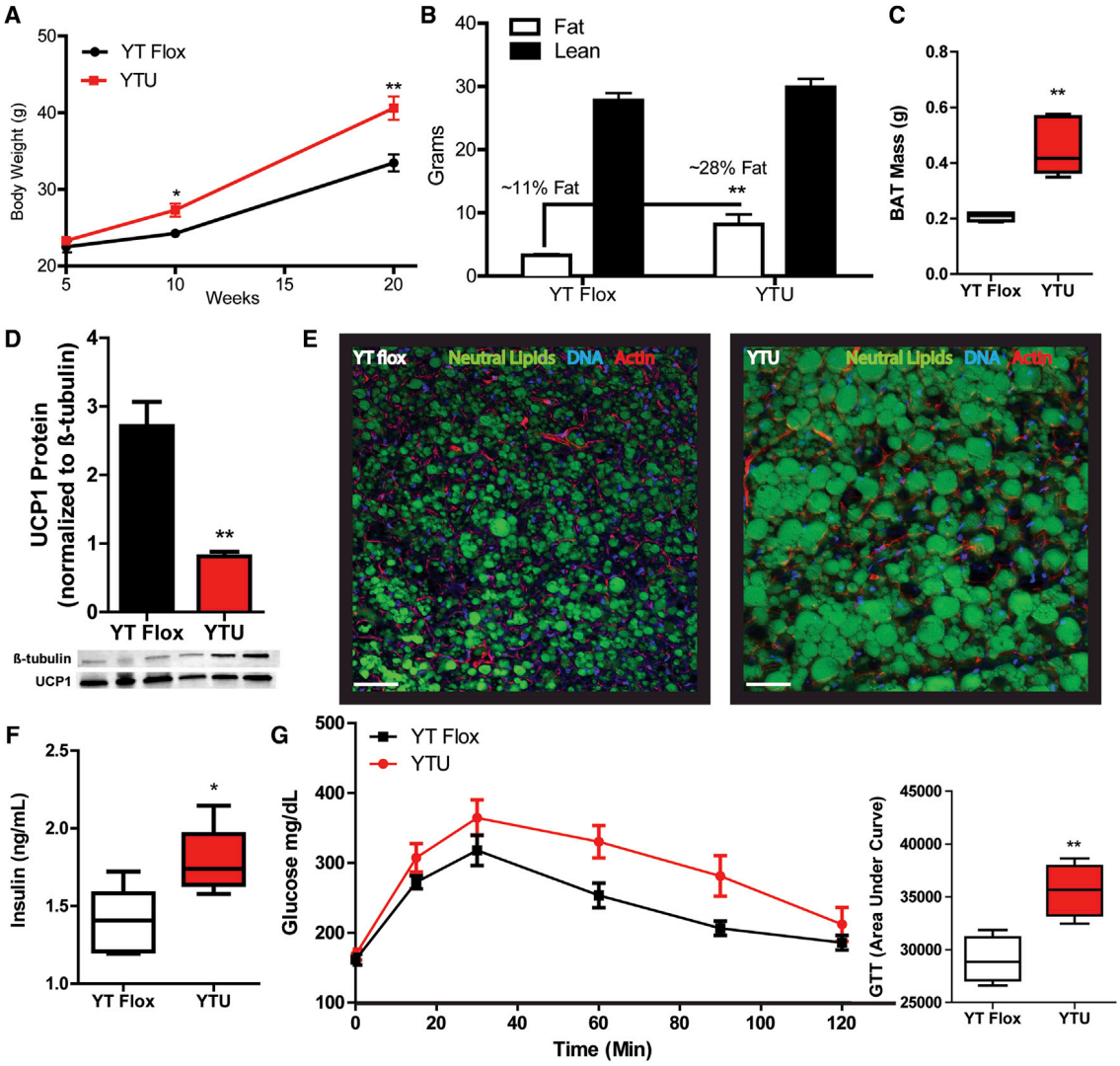

Figure 7. Influence of YAP/TAZ Regulated Thermogenic Program on Whole-Body Metabolism

(A) Body weight change of male YT Flox and YTU mice fed a normal chow diet *ad libitum* over 20 weeks with no observable differences in food consumption (n = 5).

(B) Body mass composition of 20-week-old male mice, assessed with EchoMRI (n = 5).

(C) BAT mass of 20-week-old male mice (n = 5).

(D) UCP1 protein expression levels in YTU BAT of 20-week-old male mice, normalized to β-tubulin, LI-COR Odyssey (n = 3).

(E) Representative neutral lipid (green, BODIPY 3922), nuclei/DNA (blue, DAPI), and actin (red, phalloidin) staining of BAT from 20-week-old male mice. Scale bars, 50 μm.

(F) Serum insulin concentrations (fed) from 20-week-old male mice (n = 4).

(G) Glucose tolerance test of 20-week-old male mice with area under the curve quantitated in associated bar graph (n = 4).

Error bars represent ± SEM. *p < 0.05 and **p < 0.01. See also Figure S6.

the expression patterns observed in BATs enables internally generated mechanical stimuli, which activates YAP/TAZ to support thermogenic gene expression. In addition, we have characterized a new aspect of the well-studied β-adrenergic activation of thermogenic adipocytes, uncovering a previously unknown mechanical program that is critical for metabolic flux in BAT. We propose that YAP/TAZ-mediated regulation of UCP1 expression uncovered here is basally required but operates in concert with the previously described regulators of UCP1 expression in adipose tissues such as CREB, PRDM16, PPARGC1A, and PPARG (Inagaki et al., 2016). While we do find a direct interaction of YAP with the UCP1 promoter region, evidence would suggest that the predominant effect of YAP/TAZ-TEAD is through interactions with enhancer regions throughout the genome (Galli et al., 2015; Zanconato et al., 2015), which may foster lineage-restricted reprograming of cellular phenotypes (Panciera et al., 2016).

Actomyosin-mediated mechanotransduction is well known to regulate the differentiation of MSCs through numerous mechanisms (Engler et al., 2006; Lv et al., 2015; McBeath et al., 2004; Sordella et al., 2003; Zajac and Discher, 2008). Previous studies

of YAP/TAZ and MSC differentiation have led to the description of YAP/TAZ as anti-adipogenic (Dupont et al., 2011; Hong et al., 2005). However, this conclusion may be convoluted by the culture of MSCs on supraphysiologically stiff (~3 GPa) tissue culture polystyrene (TCPS) surfaces. Adipose tissue depots possess a storage modulus roughly three orders of magnitude softer than that of TCPS, which suggests that the *in vitro* findings may be due hyperactivation of YAP/TAZ on the stiff TCPS surfaces. Mechanoregulation of MSC differentiation can be controlled by externally applied or internally generated physical stresses (Discher et al., 2005; Robinson, 2015; Schwartz, 2010; Vogel and Sheetz, 2006), making it challenging to decouple extrinsic and intrinsic responses to mechanical stimuli. To date, our study is the first to examine the role of YAP/TAZ in adipose tissue development and function *in vivo*. Our identification of YAP/TAZ as critical for BAT development certainly prompts further study of YAP/TAZ in WAT development, hypertrophy, and hyperplasia.

Chronic YAP/TAZ activity has been suggested to mediate inflammation of fibrotic adipose tissues due to the altered physical properties ECM, further demonstrating that hyperactivation of this pathway can have undesirable consequences (Zanconato et al., 2016). In fibrotic WATs, chronic mechanosensing of the aberrantly composed and crosslinked ECM enhances inflammatory cytokine profiles (Pellegrinelli et al., 2014; Sun et al., 2014), many of the same inflammatory cytokines thought to support the metabolic benefits of thermogenic adipose expansion (Stanford et al., 2013). Prevention of chronic activation of YAP/TAZ transcriptional programs is regulated by numerous self-regulated negative feedback mechanisms (Moleirinho et al., 2014; Moroishi et al., 2015b). YAP/TAZ autoregulation promotes the expression of proteins and enzymes that dictate co-factor associations and nuclear exclusion, making it challenging to define the role of YAP/TAZ in long-term disease-promoting states, such as obesity, which affects both preadipocyte and adipocyte biology.

The expression profile of the contractile signaling and infrastructure in BAT appears to strongly mimic that of cardiomyocytes. Specifically, adrenergic simulation increases cAMP levels that activate PKA to activate L-type Ca^{2+} channels to then facilitate an influx of calcium. The influx of calcium activates MYLKs to phosphorylate myosin hexamers, promoting their association with actin and ATPase activity, in turn generating tension on the actin cytoskeleton, which increases cellular elasticity. Adrenergic stimulation has also been identified to promote mitochondrial fragmentation in brown adipocytes (Wikstrom et al., 2014), which leads us to postulate that mitochondrial dynamics may require mechanical support from actomyosin. Actin dynamics have only recently been identified to modulate mitochondrial function in mammalian cells (Beck et al., 2012), and ER-associated mitochondrial divisions appear to require force generated by the actin cytoskeleton (Hatch et al., 2014; Korobova et al., 2013). While our data suggest a significant role for mechanoregulation in mitochondrial function during thermoregulation, further study is necessary to establish a mechanistic explanation of how respiration is regulated by cellular elasticity.

Importantly, we have shown a dynamic and essential role of actomyosin mechanics in thermogenic adipocytes, but it remains to be clarified what developmental signals stimulate contractile gene expression in preadipocytes. It appears that, early in adipogenesis, MSCs destined to express functional levels of UCP1 express muscle-like actomyosin machinery (Farmer, 2008; Long et al., 2014; Timmons et al., 2007) that is induced by cold exposure (Rosell et al., 2014) and interleukin-33 (Odegaard et al., 2016). Pharmacological inhibition of BAT mechanobiology, as with verapamil, may underlie previously unclear clinical side effects of this drug, such as rapid weight gain. In contrast, approaches to drive the activation of actomyosin activity in BAT may engender new approaches to combat metabolic diseases. In summary, actomyosin mechanics alter cellular elasticity profiles that provide an essential metabolic function by promoting the development of and acutely supporting the thermogenic capacity of brown and beige adipocytes.

Limitations of Study

We have yet to assess the roles of YAP and TAZ independently of each other, and with temporal control during the course of adipogenesis. Significantly more work is needed to decipher the specific roles of the various MYH species with regard to basal or stimulated cellular elasticity. This will be particularly challenging as *in vitro* models of cytoskeletal structure and function are limited in their recapitulation of *in vivo* dynamics, as organotypic structure and composition are lacking. In addition, the profound effects of blebbistatin on oxidative metabolism in adipocytes warrant extensive study. As we have highlighted, a number of publications have implicated various MYH species in lipid droplet and mitochondrial dynamics. Ultimately, we hope to assemble an integrative model of subcellular cytoskeletal dynamics and metabolic flux in thermogenic adipocytes.

STAR★METHODS

Detailed methods are provided in the online version of this paper and include the following:

- KEY RESOURCES TABLE
- CONTACT FOR REAGENT AND RESOURCE SHARING
- EXPERIMENTAL MODEL AND SUBJECT DETAILS
  - Brown and Beige Adipocyte Cell Lines
  - Mouse Models
- METHOD DETAILS
  - rtPCR
  - RNAseq
  - siRNA, YAP-GFP, and CA-MYLK
  - Immunofluorescence Microscopy
  - *In Vivo* Respirometry
  - *In Vitro* Respirometry
  - Protein Quantification and Western Blotting
  - Rheology
  - Atomic Force Microscopy
  - Gulcose Tolerance Test
  - ChIP
- QUANTIFICATION AND STATISTICAL ANALYSIS
- DATA AND SOFTWARE AVAILABILITY

SUPPLEMENTAL INFORMATION

Supplemental Information includes seven figures and two tables and can be found with this article online at https://doi.org/10.1016/j.cmet.2018.02.005.

ACKNOWLEDGMENTS

This work was supported in part by NIH grants R01DK101293 and R01DK089202, and the American Diabetes Association basic science award 1-14-BS-191 awarded to A.S. We thank the UC Berkeley imaging core facility members Denise Schichnes and Dr. Steve Ruzin for their support. Research reported in this publication was supported in part by the NIH S10 program, under award number 1S10RR026866-01. The content is solely the responsibility of the authors and does not necessarily represent the official views of the NIH. Importantly, we thank the UCSF Transgenic Mouse Facility for providing us with the $YAP^{f/f}/TAZ^{f/f}$ mice, and Dr. H.S.S. for providing us with the UCP1-Cre mice. We also thank Dr. Matthew Welch for an insightful critique and Sharad Mahajan for experimental contributions.

AUTHOR CONTRIBUTIONS

Conceptualization, K.M.T. and A.S.; Methodology, K.M.T., M.S.K., G.A.T., J.D., H.S.S., S. Kumar, K.E.H., and A.S.; Investigation, K.M.T., M.S.K., G.A.T., J.D., G.E.D., P.-J.H.Z., J.B., C.C., and C.X.L.; Supervision, A.K.J.; Resources, S. Kajimura; Writing – Original Draft, K.M.T.; Visualization, K.M.T.; Writing – Review & Editing, A.S., M.S.K., G.A.T., K.S., and S. Kumar; Funding Acquisition, K.E.H. and A.S.; Project Administration, K.M.T. and A.S.

DECLARATION OF INTERESTS

The authors declare no competing interests.

Received: June 5, 2017
Revised: October 18, 2017
Accepted: February 6, 2018
Published: March 6, 2018

REFERENCES

Anders, S., and Huber, W. (2010). Differential expression analysis for sequence count data. Genome Biol. *11*, R106.

Backx, P.H., Gao, W.D., Azan-Backx, M.D., and Marban, E. (1994). Mechanism of force inhibition by 2,3-butanedione monoxime in rat cardiac muscle: roles of [Ca2+]i and cross-bridge kinetics. J. Physiol. *476*, 487–500.

Bartelt, A., and Heeren, J. (2014). Adipose tissue browning and metabolic health. Nat. Rev. Endocrinol. *10*, 24–36.

Beck, H., Flynn, K., Lindenberg, K.S., Schwarz, H., Bradke, F., Di Giovanni, S., and Knoll, B. (2012). Serum response factor (SRF)-cofilin-actin signaling axis modulates mitochondrial dynamics. Proc. Natl. Acad. Sci. USA *109*, E2523–E2532.

Berry, D.C., Jiang, Y., and Graff, J.M. (2016). Mouse strains to study cold-inducible beige progenitors and beige adipocyte formation and function. Nat. Commun. *7*, 10184.

Bers, D.M. (2002). Cardiac excitation-contraction coupling. Nature *415*, 198–205.

Cannon, B., and Nedergaard, J. (2004). Brown adipose tissue: function and physiological significance. Physiol. Rev. *84*, 277–359.

Cao, W., Daniel, K.W., Robidoux, J., Puigserver, P., Medvedev, A.V., Bai, X., Floering, L.M., Spiegelman, B.M., and Collins, S. (2004). p38 mitogen-activated protein kinase is the central regulator of cyclic AMP-dependent transcription of the brown fat uncoupling protein 1 gene. Mol. Cell. Biol. *24*, 3057–3067.

Collins, S., Yehuda-Shnaidman, E., and Wang, H. (2010). Positive and negative control of Ucp1 gene transcription and the role of beta-adrenergic signaling networks. Int. J. Obes. *34* (*Suppl 1*), S28–S33.

Dempersmier, J., Sambeat, A., Gulyaeva, O., Paul, S.M., Hudak, C.S., Raposo, H.F., Kwan, H.Y., Kang, C., Wong, R.H., and Sul, H.S. (2015). Cold-inducible Zfp516 activates UCP1 transcription to promote browning of white fat and development of brown fat. Mol. Cell *57*, 235–246.

Discher, D.E., Janmey, P., and Wang, Y.L. (2005). Tissue cells feel and respond to the stiffness of their substrate. Science *310*, 1139–1143.

Dobin, A., Davis, C.A., Schlesinger, F., Drenkow, J., Zaleski, C., Jha, S., Batut, P., Chaisson, M., and Gingeras, T.R. (2013). STAR: ultrafast universal RNA-seq aligner. Bioinformatics *29*, 15–21.

Dolgacheva, L.P., Abzhalelov, B.B., Zhang, S.J., Zinchenko, V.P., and Bronnikov, G.E. (2003). Norepinephrine induces slow calcium signalling in murine brown preadipocytes through the beta-adrenoceptor/cAMP/protein kinase A pathway. Cell. Signal. *15*, 209–216.

Dupont, S., Morsut, L., Aragona, M., Enzo, E., Giulitti, S., Cordenonsi, M., Zanconato, F., Le Digabel, J., Forcato, M., Bicciato, S., et al. (2011). Role of YAP/TAZ in mechanotransduction. Nature *474*, 179–183.

Engler, A.J., Sen, S., Sweeney, H.L., and Discher, D.E. (2006). Matrix elasticity directs stem cell lineage specification. Cell *126*, 677–689.

Farmer, S.R. (2008). Brown fat and skeletal muscle: unlikely cousins? Cell *134*, 726–727.

Forner, F., Kumar, C., Luber, C.A., Fromme, T., Klingenspor, M., and Mann, M. (2009). Proteome differences between brown and white fat mitochondria reveal specialized metabolic functions. Cell Metab. *10*, 324–335.

Galli, G.G., Carrara, M., Yuan, W.C., Valdes-Quezada, C., Gurung, B., Pepe-Mooney, B., Zhang, T., Geeven, G., Gray, N.S., de Laat, W., et al. (2015). YAP drives growth by controlling transcriptional pause release from dynamic enhancers. Mol. Cell *60*, 328–337.

Galmozzi, A., Sonne, S.B., Altshuler-Keylin, S., Hasegawa, Y., Shinoda, K., Luijten, I.H., Chang, J.W., Sharp, L.Z., Cravatt, B.F., Saez, E., et al. (2014). ThermoMouse: an in vivo model to identify modulators of UCP1 expression in brown adipose tissue. Cell Rep. *9*, 1584–1593.

Gregoire, F.M., Smas, C.M., and Sul, H.S. (1998). Understanding adipocyte differentiation. Physiol. Rev. *78*, 783–809.

Halder, G., Dupont, S., and Piccolo, S. (2012). Transduction of mechanical and cytoskeletal cues by YAP and TAZ. Nat. Rev. Mol. Cell Biol. *13*, 591–600.

Hall, A.R., and Hausenloy, D.J. (2016). Mitochondrial respiratory inhibition by 2,3-butanedione monoxime (BDM): implications for culturing isolated mouse ventricular cardiomyocytes. Physiol. Rep. *4*, e12606.

Hansen, C.G., Moroishi, T., and Guan, K.L. (2015). YAP and TAZ: a nexus for Hippo signaling and beyond. Trends Cell Biol. *25*, 499–513.

Harms, M., and Seale, P. (2013). Brown and beige fat: development, function and therapeutic potential. Nat. Med. *19*, 1252–1263.

Hatch, A.L., Gurel, P.S., and Higgs, H.N. (2014). Novel roles for actin in mitochondrial fission. J. Cell Sci. *127*, 4549–4560.

Heinz, S., Benner, C., Spann, N., Bertolino, E., Lin, Y.C., Laslo, P., Cheng, J.X., Murre, C., Singh, H., and Glass, C.K. (2010). Simple combinations of lineage-determining transcription factors prime cis-regulatory elements required for macrophage and B cell identities. Mol. Cell *38*, 576–589.

Hill, B.G. (2015). Insights into an adipocyte whitening program. Adipocyte *4*, 75–80.

Hong, J.H., Hwang, E.S., McManus, M.T., Amsterdam, A., Tian, Y., Kalmukova, R., Mueller, E., Benjamin, T., Spiegelman, B.M., Sharp, P.A., et al. (2005). TAZ, a transcriptional modulator of mesenchymal stem cell differentiation. Science *309*, 1074–1078.

Hwang, P.M., and Sykes, B.D. (2015). Targeting the sarcomere to correct muscle function. Nat. Rev. Drug Discov. *14*, 313–328.

Inagaki, T., Sakai, J., and Kajimura, S. (2016). Transcriptional and epigenetic control of brown and beige adipose cell fate and function. Nat. Rev. Mol. Cell. Biol. *17*, 480–495.

Johnson, R., and Halder, G. (2014). The two faces of Hippo: targeting the Hippo pathway for regenerative medicine and cancer treatment. Nat. Rev. Drug Discov. *13*, 63–79.

Kajimura, S., Spiegelman, B.M., and Seale, P. (2015). Brown and beige fat: physiological roles beyond heat generation. Cell Metab. *22*, 546–559.

Kamm, K.E., and Stull, J.T. (1985). The function of myosin and myosin light chain kinase phosphorylation in smooth muscle. Annu. Rev. Pharmacol. Toxicol. *25*, 593–620.

Kamp, T.J., and Hell, J.W. (2000). Regulation of cardiac L-type calcium channels by protein kinase A and protein kinase C. Circ. Res. *87*, 1095–1102.

Korobova, F., Ramabhadran, V., and Higgs, H.N. (2013). An actin-dependent step in mitochondrial fission mediated by the ER-associated formin INF2. Science *339*, 464–467.

Kovacs, M., Toth, J., Hetenyi, C., Malnasi-Csizmadia, A., and Sellers, J.R. (2004). Mechanism of blebbistatin inhibition of myosin II. J. Biol. Chem. *279*, 35557–35563.

Leaver, E.V., and Pappone, P.A. (2002). Beta-adrenergic potentiation of endoplasmic reticulum Ca(2+) release in brown fat cells. Am. J. Physiol. Cell Physiol. *282*, C1016–C1024.

Limouze, J., Straight, A.F., Mitchison, T., and Sellers, J.R. (2004). Specificity of blebbistatin, an inhibitor of myosin II. J. Muscle Res. Cell Motil. *25*, 337–341.

Long, J.Z., Svensson, K.J., Tsai, L., Zeng, X., Roh, H.C., Kong, X., Rao, R.R., Lou, J., Lokurkar, I., Baur, W., et al. (2014). A smooth muscle-like origin for beige adipocytes. Cell Metab. *19*, 810–820.

Luque, T., and Kang, M.S. (2016). Microelastic mapping of the rat dentate gyrus. R. Soc. Open. Sci. *3*, 150702.

Lv, H., Li, L., Sun, M., Zhang, Y., Chen, L., Rong, Y., and Li, Y. (2015). Mechanism of regulation of stem cell differentiation by matrix stiffness. Stem Cell Res. Ther. *6*, 103.

Malik, F.I., Hartman, J.J., Elias, K.A., Morgan, B.P., Rodriguez, H., Brejc, K., Anderson, R.L., Sueoka, S.H., Lee, K.H., Finer, J.T., et al. (2011). Cardiac myosin activation: a potential therapeutic approach for systolic heart failure. Science *331*, 1439–1443.

McBeath, R., Pirone, D.M., Nelson, C.M., Bhadriraju, K., and Chen, C.S. (2004). Cell shape, cytoskeletal tension, and RhoA regulate stem cell lineage commitment. Dev. Cell *6*, 483–495.

McDonald, M.E., Li, C., Bian, H., Smith, B.D., Layne, M.D., and Farmer, S.R. (2015). Myocardin-related transcription factor A regulates conversion of progenitors to beige adipocytes. Cell *160*, 105–118.

Miralles, F., Posern, G., Zaromytidou, A.I., and Treisman, R. (2003). Actin dynamics control SRF activity by regulation of its coactivator MAL. Cell *113*, 329–342.

Moleirinho, S., Guerrant, W., and Kissil, J.L. (2014). The angiomotins – from discovery to function. FEBS Lett. *588*, 2693–2703.

Moroishi, T., Hansen, C.G., and Guan, K.L. (2015a). The emerging roles of YAP and TAZ in cancer. Nat. Rev. Cancer *15*, 73–79.

Moroishi, T., Park, H.W., Qin, B., Chen, Q., Meng, Z., Plouffe, S.W., Taniguchi, K., Yu, F.X., Karin, M., Pan, D., et al. (2015b). A YAP/TAZ-induced feedback mechanism regulates Hippo pathway homeostasis. Genes Dev. *29*, 1271–1284.

Nobusue, H., Onishi, N., Shimizu, T., Sugihara, E., Oki, Y., Sumikawa, Y., Chiyoda, T., Akashi, K., Saya, H., and Kano, K. (2014). Regulation of MKL1 via actin cytoskeleton dynamics drives adipocyte differentiation. Nat. Commun. *5*, 3368.

Odegaard, J.I., Lee, M.W., Sogawa, Y., Bertholet, A.M., Locksley, R.M., Weinberg, D.E., Kirichok, Y., Deo, R.C., and Chawla, A. (2016). Perinatal licensing of thermogenesis by IL-33 and ST2. Cell *166*, 841–854.

Olson, E.N., and Nordheim, A. (2010). Linking actin dynamics and gene transcription to drive cellular motile functions. Nat. Rev. Mol. Cell Biol. *11*, 353–365.

Ostap, E.M. (2002). 2,3-Butanedione monoxime (BDM) as a myosin inhibitor. J. Muscle Res. Cell Motil. *23*, 305–308.

Panciera, T., Azzolin, L., Fujimura, A., Di Biagio, D., Frasson, C., Bresolin, S., Soligo, S., Basso, G., Bicciato, S., Rosato, A., et al. (2016). Induction of expandable tissue-specific stem/progenitor cells through transient expression of YAP/TAZ. Cell Stem Cell *19*, 725–737.

Pellegrinelli, V., Heuvingh, J., du Roure, O., Rouault, C., Devulder, A., Klein, C., Lacasa, M., Clément, E., Lacasa, D., and Clement, K. (2014). Human adipocyte function is impacted by mechanical cues. J. Pathol. *233*, 183–195.

Pfisterer, S.G., Gateva, G., Horvath, P., Pirhonen, J., Salo, V.T., Karhinen, L., Varjosalo, M., Ryhanen, S.J., Lappalainen, P., and Ikonen, E. (2017). Role for formin-like 1-dependent acto-myosin assembly in lipid droplet dynamics and lipid storage. Nat. Commun. *8*, 14858.

Posern, G., and Treisman, R. (2006). Actin' together: serum response factor, its cofactors and the link to signal transduction. Trends Cell Biol. *16*, 588–596.

Radke, M.B., Taft, M.H., Stapel, B., Hilfiker-Kleiner, D., Preller, M., and Manstein, D.J. (2014). Small molecule-mediated refolding and activation of myosin motor function. Elife *3*, e01603.

Rammensee, S., Kang, M.S., Georgiou, K., Kumar, S., and Schaffer, D.V. (2017). Dynamics of mechanosensitive neural stem cell differentiation. Stem Cells *35*, 497–506.

Robinson, D.N. (2015). Molecular mechanisms of contractility-based cellular mechanosensing. Biophys. J. *108*, 4a–5a.

Robinson, M.D., McCarthy, D.J., and Smyth, G.K. (2010). edgeR: a Bioconductor package for differential expression analysis of digital gene expression data. Bioinformatics *26*, 139–140.

Rosell, M., Kaforou, M., Frontini, A., Okolo, A., Chan, Y.W., Nikolopoulou, E., Millership, S., Fenech, M.E., MacIntyre, D., Turner, J.O., et al. (2014). Brown and white adipose tissues: intrinsic differences in gene expression and response to cold exposure in mice. Am. J. Physiol. Endocrinol. Metab. *306*, E945–E964.

Sambeat, A., Gulyaeva, O., Dempersmier, J., Tharp, K.M., Stahl, A., Paul, S.M., and Sul, H.S. (2016). LSD1 interacts with Zfp516 to promote UCP1 transcription and brown fat program. Cell Rep. *15*, 2536–2549.

Schiller, Z.A., Schiele, N.R., Sims, J.K., Lee, K., and Kuo, C.K. (2013). Adipogenesis of adipose-derived stem cells may be regulated via the cytoskeleton at physiological oxygen levels in vitro. Stem Cell Res. Ther. *4*, 79.

Schulz, A.S., Glatting, G., Hoenig, M., Schuetz, C., Gatz, S.A., Grewendorf, S., Sparber-Sauer, M., Muche, R., Blumstein, N., Kropshofer, G., et al. (2011). Radioimmunotherapy-based conditioning for hematopoietic cell transplantation in children with malignant and nonmalignant diseases. Blood *117*, 4642–4650.

Schwartz, M.A. (2010). Integrins and extracellular matrix in mechanotransduction. Cold Spring Harb. Perspect. Biol. *2*, a005066.

Seale, P., Bjork, B., Yang, W., Kajimura, S., Chin, S., Kuang, S., Scime, A., Devarakonda, S., Conroe, H.M., Erdjument-Bromage, H., et al. (2008). PRDM16 controls a brown fat/skeletal muscle switch. Nature *454*, 961–967.

Shen, Y.T., Malik, F.I., Zhao, X., Depre, C., Dhar, S.K., Abarzua, P., Morgans, D.J., and Vatner, S.F. (2010). Improvement of cardiac function by a cardiac myosin activator in conscious dogs with systolic heart failure. Circ. Heart Fail. *3*, 522–527.

Sordella, R., Jiang, W., Chen, G.C., Curto, M., and Settleman, J. (2003). Modulation of Rho GTPase signaling regulates a switch between adipogenesis and myogenesis. Cell *113*, 147–158.

Stanford, K.I., Middelbeek, R.J., Townsend, K.L., An, D., Nygaard, E.B., Hitchcox, K.M., Markan, K.R., Nakano, K., Hirshman, M.F., Tseng, Y.H., et al. (2013). Brown adipose tissue regulates glucose homeostasis and insulin sensitivity. J. Clin. Invest. *123*, 215–223.

Straight, A.F., Cheung, A., Limouze, J., Chen, I., Westwood, N.J., Sellers, J.R., and Mitchison, T.J. (2003). Dissecting temporal and spatial control of cytokinesis with a myosin II Inhibitor. Science *299*, 1743–1747.

Sun, K., Park, J., Gupta, O.T., Holland, W.L., Auerbach, P., Zhang, N., Goncalves Marangoni, R., Nicoloro, S.M., Czech, M.P., Varga, J., et al. (2014). Endotrophin triggers adipose tissue fibrosis and metabolic dysfunction. Nat. Commun. *5*, 3485.

Tharp, K.M., and Stahl, A. (2015). Bioengineering beige adipose tissue therapeutics. Front. Endocrinol. (Lausanne) *6*, 164.

Timmons, J.A., Wennmalm, K., Larsson, O., Walden, T.B., Lassmann, T., Petrovic, N., Hamilton, D.L., Gimeno, R.E., Wahlestedt, C., Baar, K., et al. (2007). Myogenic gene expression signature establishes that brown and white adipocytes originate from distinct cell lineages. Proc. Natl. Acad. Sci. USA *104*, 4401–4406.

Tripathi, S., Pohl, M.O., Zhou, Y., Rodriguez-Frandsen, A., Wang, G., Stein, D.A., Moulton, H.M., DeJesus, P., Che, J., Mulder, L.C., et al. (2015). Meta- and orthogonal integration of influenza "OMICs" data defines a role for UBR4 in virus budding. Cell Host Microbe *18*, 723–735.

Vogel, V., and Sheetz, M. (2006). Local force and geometry sensing regulate cell functions. Nat. Rev. Mol. Cell Biol. *7*, 265–275.

Walden, T.B., Timmons, J.A., Keller, P., Nedergaard, J., and Cannon, B. (2009). Distinct expression of muscle-specific microRNAs (myomirs) in brown adipocytes. J. Cell. Physiol. *218*, 444–449.

Wang, W., and Seale, P. (2016). Control of brown and beige fat development. Nat. Rev. Mol. Cell Biol. *17*, 691–702.

Wikstrom, J.D., Mahdaviani, K., Liesa, M., Sereda, S.B., Si, Y., Las, G., Twig, G., Petrovic, N., Zingaretti, C., Graham, A., et al. (2014). Hormone-induced mitochondrial fission is utilized by brown adipocytes as an amplification pathway for energy expenditure. EMBO J. *33*, 418–436.

Winkelmann, D.A., Forgacs, E., Miller, M.T., and Stock, A.M. (2015). Structural basis for drug-induced allosteric changes to human beta-cardiac myosin motor activity. Nat. Commun. *6*, 7974.

Wong, S.Y., Ulrich, T.A., Deleyrolle, L.P., MacKay, J.L., Lin, J.M., Martuscello, R.T., Jundi, M.A., Reynolds, B.A., and Kumar, S. (2015). Constitutive activation of myosin-dependent contractility sensitizes glioma tumor-initiating cells to mechanical inputs and reduces tissue invasion. Cancer Res. *75*, 1113–1122.

Xin, M., Kim, Y., Sutherland, L.B., Murakami, M., Qi, X., McAnally, J., Porrello, E.R., Mahmoud, A.I., Tan, W., Shelton, J.M., et al. (2013). Hippo pathway effector Yap promotes cardiac regeneration. Proc. Natl. Acad. Sci. USA *110*, 13839–13844.

Young, D.A., Ibrahim, D.O., Hu, D., and Christman, K.L. (2011). Injectable hydrogel scaffold from decellularized human lipoaspirate. Acta Biomater. *7*, 1040–1049.

Zajac, A.L., and Discher, D.E. (2008). Cell differentiation through tissue elasticity-coupled, myosin-driven remodeling. Curr. Opin. Cell Biol. *20*, 609–615.

Zanconato, F., Cordenonsi, M., and Piccolo, S. (2016). YAP/TAZ at the roots of cancer. Cancer Cell *29*, 783–803.

Zanconato, F., Forcato, M., Battilana, G., Azzolin, L., Quaranta, E., Bodega, B., Rosato, A., Bicciato, S., Cordenonsi, M., and Piccolo, S. (2015). Genome-wide association between YAP/TAZ/TEAD and AP-1 at enhancers drives oncogenic growth. Nat. Cell Biol. *17*, 1218–1227.

STAR★METHODS

KEY RESOURCES TABLE

REAGENT or RESOURCE	SOURCE	IDENTIFIER
Antibodies		
UCP1	Cell Signaling	14670; RRID: AB_2687530
UCP1	Sigma	U6382; RRID: AB_261838
YAP	Abcam	EP1674Y; RRID: AB_2241957
YAP	Santa Cruz Biotech	SC-271134; RRID: AB_10612397
YAP-pSer127	Cell Signaling	4911; RRID: AB_2218913
MyH7	Sigma	SAB2106550
MyH7	Santa Cruz Biotech	SC-53089; RRID: AB_2147281
MyH11	Santa Cruz Biotech	SC-6956; RRID: AB_670119
Donkey anti Rabbit (647)	Thermo Fisher	A31573
Donkey anti Rabbit (488)	Thermo Fisher	A21206
Donkey anti Mouse (555)	Thermo Fisher	A31570
Donkey anti Mouse (647)	Thermo Fisher	A31571
F(ab')2-Goat anti-Mouse (488)	Thermo Fisher	A11017
Phalloidin (488)	Thermo Fisher	A12379
Phalloidin (647)	Thermo Fisher	A22287
CREB	Cell Signaling	9197; RRID: AB_331277
p-CREB	Cell Signaling	9198; RRID: AB_2561044
TAZ	BD Biosciences	M2-616; RRID: AB_1645338
β-tubulin	DSHB	e7; RRID: AB_528499
GAPDH	Millipore	MAP374; RRID: AB_2107445
Goat anti Mouse (680 LT)	LiCor	925-68020
Goat anti Rabbit (800 CW)	LiCor	925-32211
Bacterial and Virus Strains		
CA-MYLK tet-off	(Wong et al., 2015).	N/A
CA-MYLK tet-off control vector venus GFP	(Wong et al., 2015).	N/A
Chemicals, Peptides, and Recombinant Proteins		
LatrunculinB	Millipore	428020
Blebbistatin (racemic mixture)	Millipore	203389
EMD57003	Millipore	530657
Omecamtiv mecarbil (CK-1827452)	Selleckchem	S2623
ML7	Tocris	4310
Verapamil	Sigma	V4629
Isoproterenol	Sigma	I6504
Oligomycin	Millipore	495455
FCCP	Sigma	C2920
AntimycinA	Sigma	A8674
Rotenone	Sigma	R8875
Deposited Data		
BAT vs visceral WAT RNAseq	This paper	GEO: GSE109829
Brown adipocytes treated with blebbistatin	This paper	GEO: GSE109829
Experimental Models: Cell Lines		
Brown Adipose Cell Line	(Galmozzi et al., 2014).	N/A
Subcutaneous White Adipose Cell Line	(Galmozzi et al., 2014).	N/A
FBS used in cell culture experiments (Lot#: 378754)	Gibco	10437

(*Continued on next page*)

Continued

REAGENT or RESOURCE	SOURCE	IDENTIFIER
Experimental Models: Organisms/Strains		
Mus musculus C57BL6/J	Jackson Labs	N/A
Mus musculus C57BL6/N	Charles River	N/A
Mus musculus FVB/NL	Jackson Labs	N/A
Mus musculus b6 $Yap^{flox/flox}$:$Taz^{flox/flox}$:$R26^{mTmG/+}$	UCSF	N/A
Oligonucleotides		
Scrambled siRNA	Sigma	SIC001
YAP siRNA	Sigma	EMU088231
MYLK siRNA	Sigma	EMU061601
MyH7	Santa Cruz Biotech	SC-106222
CUGGUCAGAGAUACUUCUU dTdT (YAP)	(Zanconato et al., 2015).	N/A
AGGUACUUCCUCAAUCACA dTdT (TAZ),	(Zanconato et al., 2015).	N/A
GGCCGAUUUGUAUACCGAA dTdT (TEAD1),	(Zanconato et al., 2015).	N/A
CCUGGUGAAUUUCUUGCACAA dTdT (TEAD2),	(Zanconato et al., 2015).	N/A
UACCUUGCUCUCAAUCUGGAG dTdT (TEAD3),	(Zanconato et al., 2015).	N/A
UUUCCUGCACACACGUCUCUU dTdT (TEAD4)	(Zanconato et al., 2015).	N/A
UCP1 1878/1950 F: TCC TTT CAA TCC GGC TGT GC	This paper	N/A
1878/1950 R: TCG GAG GTG GTT AGT AGG GT	This paper	N/A
UCP1 1870/1955 F: CTG TCT CCT TTC AAT CCG GC	This paper	N/A
UCP1 1870/1955 R: GAG AGG TAT CGG AGG TGG TT	This paper	N/A
rtPCR primers	IDT	See Table S2
Recombinant DNA		
YAP-GFP	(Rammensee et al., 2017)	N/A
Venus-GFP (YAP-GFP control vector)	(Rammensee et al., 2017)	N/A
Software and Algorithms		
STAR	(Dobin et al., 2013)	N/A
DESeq	(Anders and Huber, 2010)	N/A
Metascape	(Tripathi et al., 2015)	N/A
HOMER	(Heinz et al., 2010)	N/A
Zen	Zeiss	Version 2.1
Imaris	Bitpane	Version 7

CONTACT FOR REAGENT AND RESOURCE SHARING

Further information and requests for reagents should be directed to the Lead Contact, Andreas Stahl (astahl@berkeley.edu).

EXPERIMENTAL MODEL AND SUBJECT DETAILS

Brown and Beige Adipocyte Cell Lines

Cells were maintained in DMEM with 10% serum and 1% penicillin/streptomycin (p/s) (Gibco), and induced to differentiate with the maintenance media fortified with 5 μg/ml Insulin, 1 nM T3, 2 μg/ml Dexamethasone, and 500 μM IBMX (Sigma), and 100 nM rosiglitazone (beige cells). After 3 days of differentiation media cells were maintained in DMEM with 10% serum, 1% p/s. Cells were considered fully differentiated on day 6 of differentiation as they stably expressed BAT comparable levels of UCP1, (UCP1-GAPDH ΔCT of ~2-3). Experiments assessing effects during differentiation were performed on d4-d6 of differentiation (48 h), specifically MyH7 knockdown, MYLK knockdown, and CA-MYLK expression experiments. Experiments assessing whether or not transient expression or activation effected fully differentiated cells were performed on d7-d8 of differentiation (24 h), specifically YAP/TAZ knockdown, YAP overexpression, and TEAD1-4 knockdown. Transfection/knockdown efficiency was either assessed by rtPCR for target genes or assessment of % GFP-positive cells per field view.

Mouse Models

YAP-LoxP and TAZ-LoxP mice (Xin et al., 2013) and UCP1-Cre mice (Dempersmier et al., 2015; Sambeat et al., 2016). Data depicts the comparison of YAP/TAZ flox (YT Flox) allele control animals relative to heterozygous UCP1-Cre YAP/TAZ flox allele mice (YTU).

METHOD DETAILS

rtPCR

mRNA was isolated from tissues or *in vitro* cultures with TRIzol reagent (Ambion). Tissue samples were homogenized with a Polytron PT 2100. Assays were carried out on an ABI 7500 RT-PCR system with TaqMan Universal Master Mix II and validated PrimeTime primer probe sets that detect all splice variants (Integrated DNA Technologies). A first-strand cDNA synthesis kit (Fisher) was used to transcribe 5 μg RNA/20 μL. cDNA (100 ng) was used per RT-PCR reaction in triplicates. The ΔΔCT method was used to comparatively assess mRNA quantity. Primer sequences listed in Table S2.

RNAseq

Libraries were prepared from total RNA isolated with TRIzol reagent (Ambion) (3 biological replicates per condition) using Stranded mRNA-seq Kit (KAPA) and NEXTFlex barcoded adaptors (Bioo Scientific). Multiplexed samples were sequenced on an Illumina HiSeq2500 in Rapid Run mode, and reads were mapped to the mouse genome (mm9 build) using STAR (Dobin et al., 2013). EdgeR (Robinson et al., 2010) was used to identify differentially expressed transcripts, and Metascape (Tripathi et al., 2015) or HOMER (Heinz et al., 2010) was used for gene ontology and *de novo* motif finding.

siRNA, YAP-GFP, and CA-MYLK

1 μg or 500 ng of siRNA or YAP-GFP (Rammensee et al., 2017) was diluted in Lipofectamine 3000 and applied per well of differentiated cells on day 7 of differentiation or during differentiation for 48 h on day 4 to day 6 of differentiation (1 μg for 12 well format, 500 ng for seahorse XF24 plates). Sequences listed in the Key Resources Table. CA-MYLK tet-off treatment occurred on day 4 to day 6 of differentiation as previously described (Wong et al., 2015).

Immunofluorescence Microscopy

Cells or tissues were fixed in 4% paraformaldehyde for 30 min at room temperature, washed and blocked with a blocking buffer (HBSS fortified with: 10% FBS, 0.1% BSA, 0.05% saponin, and 0.1% Tween20). Primary antibodies [1:100-1:200] (see Key Resources Table) for 2 h at RT or 24 h at 4°C, Secondary antibodies [1:1000] (see Key Resources Table) for 2 h at RT. Samples were imaged with a Zeiss 710 confocal microscope and Zeiss Zen software.

In Vivo Respirometry

Oxygen consumption was measured with the Oxymax-Comprehensive Laboratory Animal Monitoring System (Columbus Instruments). Measurements were taken over the course of 12, 24, or 48 h periods. Activity was monitored in 1 min intervals of infrared beam breaks in X, Y and Z-axis and found to be not significantly different for any of the groups.

In Vitro Respirometry

Oxygen consumption was performed on fully differentiated brown adipocytes (on day 6-8 of differentiation) with the Agilent Seahorse XF24 cellular respirometer. Mitochondrial stress tests were performed on non-permeablized brown adipocytes at 100% confluence (~100k cells/well) in V28 microplates, with XF assay medium supplemented with 1 mM pyruvate (Gibco), 2 mM glutamine (Gibco), and 25 mM glucose (Sigma) at pH 7.4 and sequential additions via injection ports of Oligomycin [1 μM final], FCCP [1 μM final], and Antimycin A/Rotenone [1 μM final] during respirometry (concentrated stock solutions solubilized in 100% ethanol [2.5 mM] for mitochondrial stress test compounds). Normalized OCR values presented per stage of mitochondrial stress test of directly comparable control conditions (vehicle or scrambled siRNA relative to compound or target siRNA respectively) with non-mitochondrial oxygen consumption deducted.

Protein Quantification and Western Blotting

Pierce BCA kit, Invitrogen Novex 4-20 tris-glycine gels or Bio-RAD Protean-TGX gels, Invitrogen iBlot transfer system or Bio-Rad Transblot turbo (high MW transfer), and Li-Cor Odyssey with CREB (Cell Signaling 9197), pCreb (Cell Signaling 9198), Anti MyH7 (sc-53089), anti-YAP (Cell Signaling 4912, and SC-271134), anti-TAZ (BD biosciences M2-616), UCP1 (Sigma U6382), UCP1 (Cell Signaling 14670), and normalization to anti β-tubulin (e7 clone, DSHB) or GAPDH (Sigma 636571) with IR secondary antibodies (LiCor goat anti-mouse 680 LT, and LiCor goat anti-rabbit 800), signal intensity with LiCor Odyssey software. 5-25 μg protein loaded per lane, depending on the target or condition to prevent saturation of signal intensity.

Rheology

Viscoelastic properties of tissues were determined using an oscillatory rheometer with parallel-plate geometry (8 mm) and a gap height of 0.2 mm under 10% constant strain and frequency ranging from 0.1 Hz to 10 Hz at 37°C in a humidity-controlled chamber.

Tissues were either 1) extracted, placed in PBS, and measured within 2 h of extraction or 2) extracted, decellularized with 1% SDS in PBS for 48 h (Young et al., 2011), rinsed with fresh PBS and measured.

Atomic Force Microscopy

Indentation measurements were performed with a NanoScope Catalyst (Bruker Corporation, Billerica, MA) atomic force microscope on an inverted optical microscope (Eclipse Ti-E, Nikon Corporation, Chiyoda, Tokyo). Singe cell measurements: PFQNM-LC-A-CAL (Bruker Corporation), with manufacturer measured spring constants between 0.09 - 0.10 N/m and a half-spherical (65 nm radius) tip geometry. Force volumes with indentations of < 1 μm were taken in a 30 μm x 30 μm grid with 16 measurements per line at a frequency of 0.3Hz on fully differentiated adipocyte monolayers under basal media conditions or supplemented with 1 μM isoproterenol, 100 μM blebbistatin, or 1 mM 2,3-BDM. Tissue level measurements: Bruker MLCT-BIO - Specs: 35 degree half angle, 20 nm nominal radius, nominal spring constant ~0.01 N/m. Spring constant was calibrated before each experiment by thermal tune (7 kHz resonant frequency) (Luque and Kang, 2016). Force volumes with indentations of < 1 μm were taken in a 100 μm x 100 μm grid under basal media supplemented with 1 μM isoproterenol. For time-lapse experiments, force volumes were acquired continuously for the experimental duration. Data were analyzed using Bruker Nanoscope Analysis v1.7 software. Force curves from cytoplasmic regions of measured cells, defined as the softest zones and verified by brightfield microscopy, and from cortical regions, defined as the stiffest zones, were fitted to the Hertz contact model for a sphere indenting an infinite half-plane. We assumed a nominal Poisson's ratio of 0.3, and fit the model to the extension curve to determine Young's modulus for each force curve.

Gulcose Tolerance Test

Glucose was administered at 2 mg/g lean body mass via intraperitoneal injection to mice fasted for 6 hr. Blood glucose was measured at indicated time points with a Nova Max glucometer through a micro-incision into the tail vein.

ChIP

sBAT cells were treated with either Blebbostatin (24 h), Isoproterenol (2 h), or vehicle, washed once with RT dPBS, and crosslinked with 1% formaldehyde for 10min in fixing buffer (TruChIP Chromatin shearing kit- Covaris). Samples were processed according to the manufacturer recommended protocol and sheared on a Covaris S220 to DNA fragments <350bp. 10 μg of chromatin was precleared and incubated with 10μl YAP antibody or IgG overnight with rotation. Complexes were pulled down with 20 μl Magna ChIP A/G beads (Millipore), washed 3 times with ChIP binding buffer and once with buffer supplemented with 350mM NaCl, and eluted in elution buffer containing 0.2% SDS and 0.1 M NaHCO3. Samples were digested with 10 ug of Proteinase K and DNA was extracted using PCR cleanup (Thermo). Samples were analyzed by qPCR using UCP1 1878/1950 F: TCC TTT CAA TCC GGC TGT GC and 1878/1950 R: TCG GAG GTG GTT AGT AGG GT, as well as UCP1 1870/1955 F: CTG TCT CCT TTC AAT CCG GC and UCP1 1870/1955 R: GAG AGG TAT CGG AGG TGG TT.

QUANTIFICATION AND STATISTICAL ANALYSIS

All data are presented as SEM analyzed using Prism (GraphPad). Statistical significance was determined by either one-way ANOVA followed by Tukey posttest for the comparison of multiple conditions, or unpaired two-tailed Student t test for the comparison of two conditions. Significance presented at $P^{*} < 0.05$, $P^{**} < 0.01$, and $P^{***} < 0.001$.

DATA AND SOFTWARE AVAILABILITY

The accession number for the BAT vs. visceral WAT and brown adipocytes treated with blebbistatin RNAseq datasets reported in this paper is GEO: GSE109829.